Cell

Synthetic lethality-mediated precision oncology via the tumor transcriptome

Graphical abstract

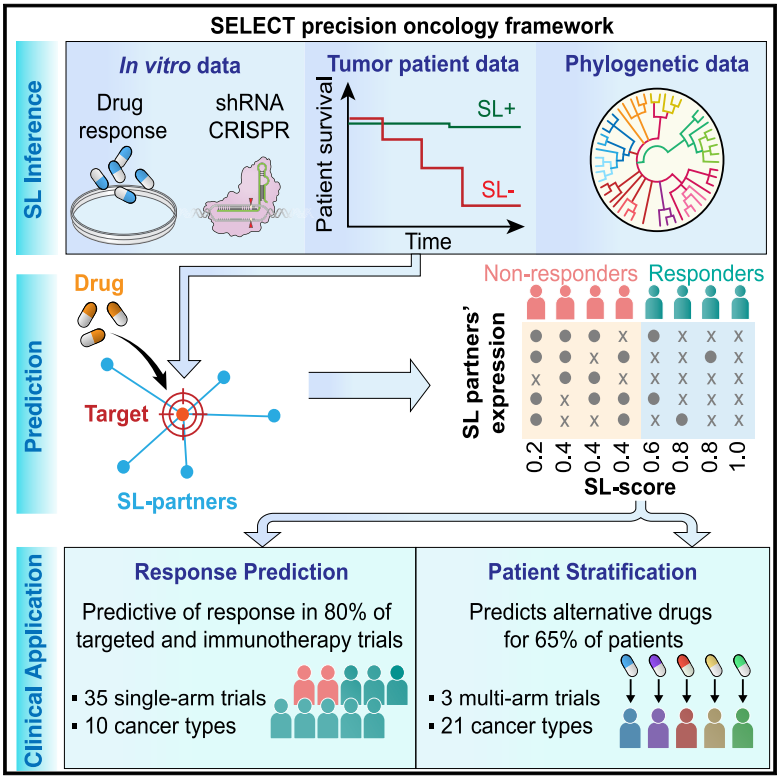

Highlights

- SELECT uses synthetic lethality and tumor transcriptome to advance precision oncology
- SELECT predicts therapy response in 28 of the 35 targeted and immunotherapy trials
- SELECT facilitates cancer patient stratification in transcriptomic multi-arm trials

Authors

Joo Sang Lee, Nishanth Ulhas Nair, Gal Dinstag, ..., Se-Hoon Lee, Kenneth Aldape, Eytan Ruppin

Correspondence

joosang.lee@skku.edu (J.S.L.), eytan.ruppin@nih.gov (E.R.)

In brief

SELECT is a precision oncology framework to analyze the tumor transcriptome. The synthetic lethal partners of drug targets are predictive of patients' response to targeted and immunotherapies across a large number of clinical trials.

Lee et al., 2021, Cell *184*, 1–16
April 29, 2021
https://doi.org/10.1016/j.cell.2021.03.030

CellPress

Please cite this article in press as: Lee et al., Synthetic lethality-mediated precision oncology via the tumor transcriptome, Cell (2021), https://doi.org/10.1016/j.cell.2021.03.030

Cell

CellPress

Theory

Synthetic lethality-mediated precision oncology via the tumor transcriptome

Joo Sang Lee,[1,2,3,*] Nishanth Ulhas Nair,[1] Gal Dinstag,[4] Lesley Chapman,[1] Youngmin Chung,[2] Kun Wang,[1] Sanju Sinha,[1] Hongui Cha,[3] Dasol Kim,[2] Alexander V. Schperberg,[5] Ajay Srinivasan,[6] Vladimir Lazar,[7] Eitan Rubin,[8] Sohyun Hwang,[9] Raanan Berger,[10] Tuvik Beker,[4] Ze'ev Ronai,[11] Sridhar Hannenhalli,[1] Mark R. Gilbert,[12] Razelle Kurzrock,[7,13] Se-Hoon Lee,[3,14] Kenneth Aldape,[15] and Eytan Ruppin[1,16,*]

[1]Cancer Data Science Lab, Center for Cancer Research, National Cancer Institute, National Institutes of Health, Bethesda, MD 20892, USA
[2]Next Generation Medicine Lab, Department of Artificial Intelligence & Department of Precision Medicine, School of Medicine, Sungkyunkwan University, Suwon 16419, Republic of Korea
[3]Department of Digital Health & Health Sciences and Technology, Samsung Advanced Institute for Health Sciences & Technology, Samsung Medical Center, Sungkyunkwan University, Seoul 06351, Republic of Korea
[4]Pangea Therapeutics, Ltd., Tel Aviv 6971003, Israel
[5]Department of Mechanical and Aerospace Engineering, University of California, Los Angeles, Los Angeles, CA 90095, USA
[6]Research and Innovations Group, Datar Cancer Genetics Limited, Nasik, Maharashtra 422010, India
[7]Worldwide Innovative Network (WIN) Association-WIN Consortium, Villejuif 94801, France
[8]The Center for Evolutionary Genomics and Medicine, Ben-Gurion University of the Negev, Beersheva 8410501, Israel
[9]Department of Pathology, CHA University, CHA Bundang Medical Center, Seongnam 13497, Republic of Korea
[10]Cancer Center, Chaim Sheba Medical Center, Tel Hashomer 5262000, Israel
[11]Cancer Center, Sanford Burnham Prebys Medical Discovery Institute, La Jolla, CA 92037, USA
[12]Neuro-Oncology Branch, Center for Cancer Research, National Cancer Institute, National Institutes of Health, Bethesda, MD 20892, USA
[13]Moore Cancer Center, University of California, San Diego, San Diego, CA 92037, USA
[14]Division of Hematology-Oncology, Department of Medicine, Samsung Medical Center, Sungkyunkwan University School of Medicine, Seoul 06351, South Korea
[15]Laboratory of Pathology, Center for Cancer Research, National Cancer Institute, National Institutes of Health, Bethesda, MD 20892, USA
[16]Lead contact
*Correspondence: joosang.lee@skku.edu (J.S.L.), eytan.ruppin@nih.gov (E.R.)
https://doi.org/10.1016/j.cell.2021.03.030

SUMMARY

Precision oncology has made significant advances, mainly by targeting actionable mutations in cancer driver genes. Aiming to expand treatment opportunities, recent studies have begun to explore the utility of tumor transcriptome to guide patient treatment. Here, we introduce SELECT (synthetic lethality and rescue-mediated precision oncology via the transcriptome), a precision oncology framework harnessing genetic interactions to predict patient response to cancer therapy from the tumor transcriptome. SELECT is tested on a broad collection of 35 published targeted and immunotherapy clinical trials from 10 different cancer types. It is predictive of patients' response in 80% of these clinical trials and in the recent multi-arm WINTHER trial. The predictive signatures and the code are made publicly available for academic use, laying a basis for future prospective clinical studies.

INTRODUCTION

There have been significant advances in precision oncology, with an increasing adoption of sequencing tests that identify targetable mutations in cancer driver genes. Aiming to complement these efforts by considering genome-wide tumor alterations at additional "-omics" layers, recent studies have begun to explore the utilization of transcriptomics data to guide cancer patients' treatment (Beaubier et al., 2019; Hayashi et al., 2020; Rodon et al., 2019; Tanioka et al., 2018; Vaske et al., 2019; Wong et al., 2020). These studies have reported encouraging results, testifying to the potential of such approaches to complement mutation panels and increase the likelihood that patients will benefit from genomics-guided precision treatments. However, current approaches for utilizing tumor transcriptomics data to guide patient treatments are still of heuristic exploratory nature, raising the need for developing and testing new systematic approaches.

Here, we present a precision oncology framework, SELECT (synthetic lethality and rescue-mediated precision oncology via the transcriptome), aimed at selecting the best drugs for a given patient based on the tumor transcriptome. Unlike recent transcriptome-based approaches that are focused on matching drugs based on the expression of their targets (Beaubier et al.,

Please cite this article in press as: Lee et al., Synthetic lethality-mediated precision oncology via the tumor transcriptome, Cell (2021), https://doi.org/10.1016/j.cell.2021.03.030

2019; Rodon et al., 2019), our approach is based on identifying and utilizing the broader scope of genetic interactions (GIs) of drug targets, which provide biologically testable biomarkers for therapy response prediction. We focus on two major types of GIs that are highly relevant to predicting the response to cancer therapies: (1) synthetic lethal (SL) interactions that describe the relationship between two genes whose concomitant inactivation, but not their individual inactivation, reduces cell viability (e.g., an SL interaction that is widely used in the clinic is poly(ADP-ribose)polymerase [PARP] inhibitors on the background of disrupted DNA repair) (Lord and Ashworth, 2017); and (2) synthetic rescue (SR) interactions that denote a type of GIs wherein a change in the activity of one gene reduces the cell's fitness, but an alteration of another gene's activity (termed its SR partner) rescues cell viability (e.g., the rescue of Myc alterations by BCL2 activation in lymphomas [Eischen et al., 2001]). These SR interactions are of interest because when a gene is targeted by a small-molecule inhibitor or an antibody, the tumor may respond by up- or downregulating its rescuer gene(s), conferring resistance to therapies.

To identify the SL and SR partners of cancer drugs, we leverage on our two recently published computational pipelines (Lee et al., 2018; Sahu et al., 2019) that identify genetic dependencies that are supported by multiple layers of omics data, including *in vitro* functional screens, patient tumor DNA and RNA-sequencing (RNA-seq) data, and phylogenetic profile similarity across multiple species. Applying these pipelines, we have previously successfully identified a Gq-driver mutation as marker for FAK inhibitor SL treatment in uveal melanoma (Feng et al., 2019) and a synergistic SL combination for treating melanoma and pancreatic tumors with asparaginase and mitogen-activated protein kinase (MAPK) inhibitors (Pathria et al., 2019). We also identified SR interactions that mediate resistance to checkpoint therapies in melanoma (Sahu et al., 2019). However, the fundamental question of whether genetic dependencies inferred from multi-omics tumor data can be used to determine efficacious therapeutics for individual cancer patients has not been addressed so far. Here, we present and study a computational framework, termed SELECT, to address this challenge. The end result is a systematic approach for robustly predicting patients' response to targeted and immune therapies across tens of different treatments and cancer types, offering an alternative way to complement existing mutation-based approaches.

RESULTS

Overview of the SELECT framework and the analysis

We collected cancer patient pre-treatment transcriptomics profiles together with therapy response information from numerous publicly available databases, surveying Gene Expression Omnibus (GEO), ArrayExpress, and the literature, and a new unpublished cohort of anti-PD1 treatment in lung adenocarcinoma. Overall, we could find 48 such datasets that include both transcriptomics and clinical response data of 3,925 cancer patients, spanning 13 chemotherapy, 14 targeted therapy, and 21 immunotherapy datasets across 13 different cancer types. For the datasets composed of multiple treatments or placebo arms, we studied the patients receiving the specific therapy of interest. This test collection is at a scale surpassing all previous efforts to predict *patients' response* to anti-cancer treatments, at least to our knowledge (Table S1; the transcriptomics profiles and the treatment outcome information are publicly available for the 23 of 48 datasets and those are made accessible; see Data and code availability).

The SELECT framework consists of two basic steps: (A) For each drug whose response we aim to predict, we first identify the clinically relevant pan-cancer GIs (the interactions found to be shared across many cancer types) of the drug's target genes (Law et al., 2014). (B) The identified GI partners of the drug emerging from step A are then used to predict a given patient's response to a given treatment based on her/his tumor's gene expression (see Figures 1A and 1B and the STAR Methods for a complete description of this process for both SL and SR interactions, the latter of which was used to predict response to immune checkpoint therapy). The prediction of response to targeted and chemotherapy drugs is based on the SL partners of the drug targets, while the prediction of response to checkpoint therapy is based on the SR partners of these drugs' targets.

Here, we provide a short overview of the SL and SR pipelines, as follows:

(Section A in STAR Methods) Identifying SL interaction partners of drug targets (Figure 1A). (A.1) Following a modified version of ISLE (Lee et al., 2018), we begin by generating an initial pool of SL drug target interactions for targeted therapy. For each drug, we compile a list of initial candidate SL pairs of its targets by analyzing cancer cell line dependencies with RNAi, CRISPR/Cas9, or pharmacological inhibition (Aguirre et al., 2016; Barretina et al., 2012; Basu et al., 2013; Cheung et al., 2011; Cowley et al., 2014; Iorio et al., 2016; Marcotte et al., 2012, 2016; Tsherniak et al., 2017). Among these candidate SL pairs, we select those that are more likely to be clinically relevant by analyzing The Cancer Genome Atlas (TCGA) data, identifying pairs that are significantly associated with better patient survival. Finally, among the candidate pairs that remain after these two steps, we select those pairs that are supported by a phylogenetic profiling analysis (Lee et al., 2018). The top significant SL partners that pass all these filters form the candidate pool of SL partners of the specific drug in hand. However, this typically results in hundreds of significant candidate GI partners for each drug, a number that needs to be markedly reduced to obtain generalizable and biologically meaningful biomarker stratification signatures. (A.2) In the second step, SELECT generates a reduced set of interaction partners to make therapy response predictions, by choosing the top 25 SL pairs found as the compact SL signature of each drug. This number of optimal SL set size is based on a minimal amount of supervised learning performed analyzing just one single targeted dataset, as described in detail in STAR Methods. The following step describes how these SL pairs are then used to predict the response of a given patient to targeted therapies.

(Section B in STAR Methods) Predicting drug response in patients using the drug's SL partners identified in step A (Figure 1B). The SL partners of the drug identified in step A are then used to predict a given patient's response to a given treatment based on her/his tumor's gene expression. This is based on the notion that a drug will be more effective against the tumor when its SL

Please cite this article in press as: Lee et al., Synthetic lethality-mediated precision oncology via the tumor transcriptome, Cell (2021), https://doi.org/10.1016/j.cell.2021.03.030

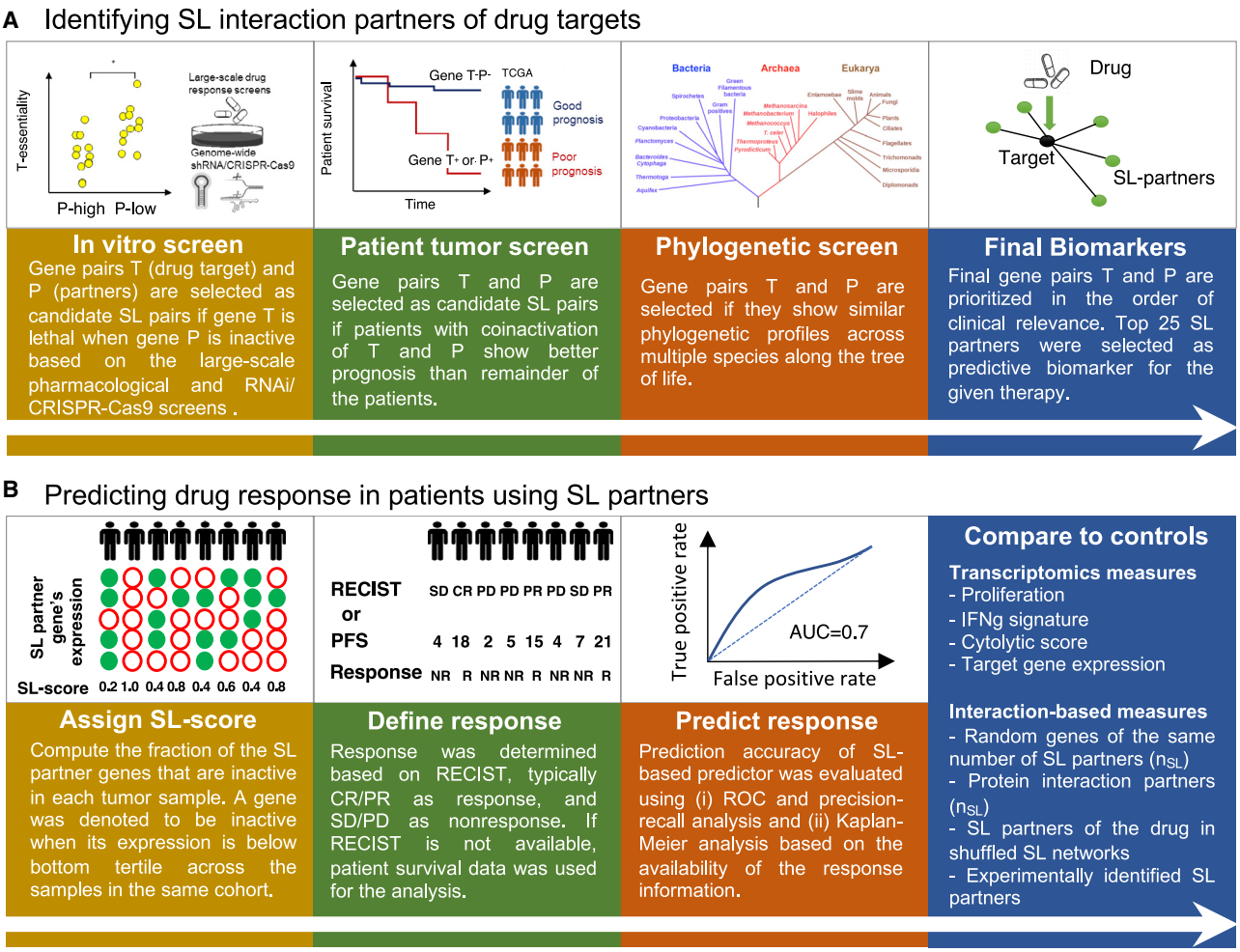

Figure 1. SELECT precision oncology framework

(A and B) The SELECT precision oncology framework is composed of two steps: (1) identifying SL interaction partners of drug targets and (2) predicting drug response in patients using SL partners. (A) The SL partners (gene P) of the drug target genes (gene T) are supported by genetic dependencies in cell lines, patient tumor data, and phylogenetic profiles. (B) The identified SL partners of the drug target genes are used to compute an SL-score to predict the response to the given therapy. See also Figures S1, S2, and Table S2.

partners are downregulated, because when the drug inhibits its targets, more SL interactions will become jointly downregulated and hence "activated." To quantify the extent of such predicted lethality, we assign an SL-score denoting the fraction of downregulated SL partners of a drug in a given tumor (STAR Methods). The larger the fraction of SL partners that are downregulated, the higher the SL-score and the more likely the patient is predicted to respond to the given therapy. Predictions of patient response to checkpoint therapy are based on SR pairs of the drug targets, which yield a stronger signal than their SL partners in this case. The process to infer the SR pairs of drugs and then their SR-scores in each patient is conceptually analogous to the process described above for targeted therapies (focusing on the top 10 pairs). The SR-score of a drug in a given patient quantifies the fraction of its downregulated SR partner genes based on the patient's tumor transcriptomics and hence the likelihood of resistance to the given therapy (STAR Methods). In defining responders versus non-responders, in all predictions made we followed the criteria used in each of the clinical trials, as explicitly listed in Table S1. In most cases, we take CR and PR as responders and SD and PD as non-responders, but there are some exceptions in cohorts where the number of samples is unevenly distributed or the response was not evaluated based on response evaluation criteria in solid tumors (RECIST) criteria, as detailed in STAR Methods and Table S1.

We emphasize that the SL/SR partners were inferred only once analyzing cancer cell line and TCGA data, and their set size was optimized by training on only one single clinical trial dataset, prior to their application to a large collection of other test clinical trial datasets (STAR Methods). In other words, the transcriptomic profiles and treatment outcome data available in all the independent test clinical trial cohorts were never used in the SL and SR inference; hence, the latter serve as independent test sets (Figure 1B). Importantly, throughout the study, we used the same fixed sets of parameters in making the predictions for targeted and immunotherapies. Taken together, these

Please cite this article in press as: Lee et al., Synthetic lethality-mediated precision oncology via the tumor transcriptome, Cell (2021), https://doi.org/10.1016/j.cell.2021.03.030

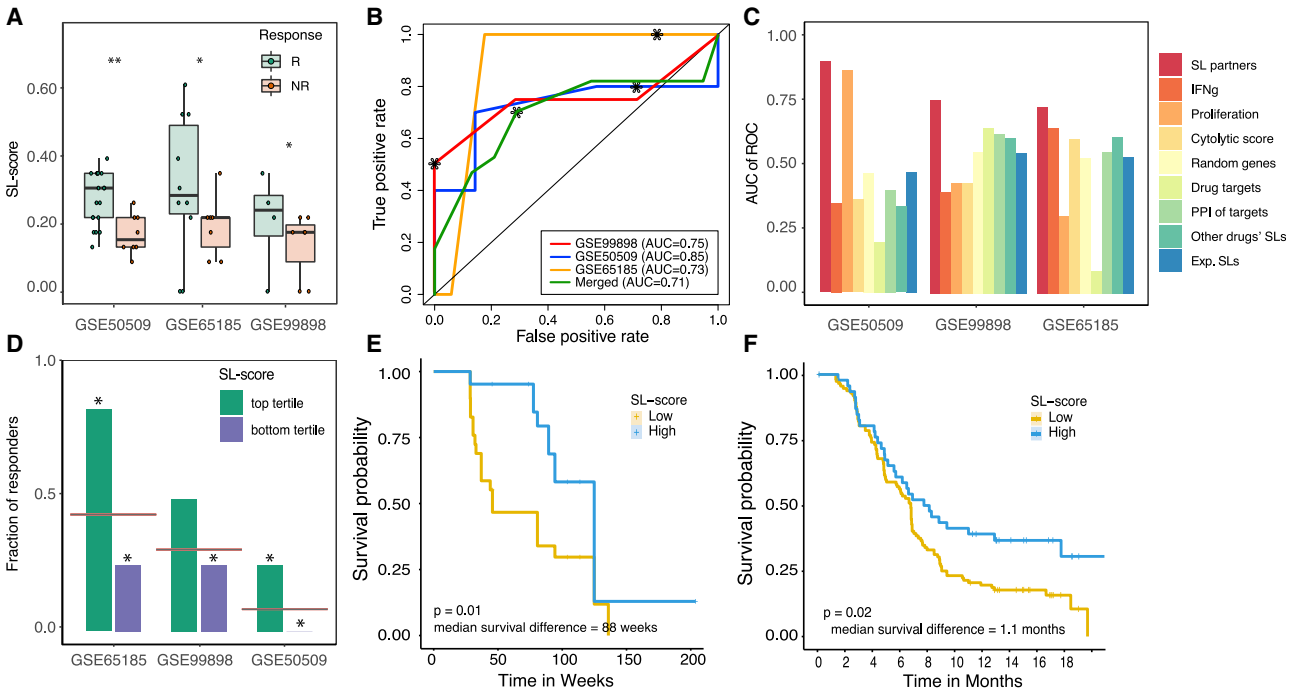

Figure 2. SELECT stratifies melanoma patients for BRAF inhibitors based on the expression of BRAF SL partners

(A) SL-scores are significantly higher in responders (green) versus non-responders (red) based on Wilcoxon rank-sum test after multiple hypothesis correction. For false discovery rates, * denotes 10% and ** denotes 5%.

(B) ROC curves depicting the prediction accuracy of the response to BRAF inhibition using SL-scores in the three melanoma cohorts (red, yellow, blue) and their aggregation (green). The stars denote the point of the maximal F1-score.

(C) Bar graphs show the predictive accuracy in terms of area under the curve (AUC) of ROC curve (y axis) of SL-based predictors (red) and controls including several known transcriptomics-deduced metrics (IFNγ signature, proliferation index, cytolytic score, and the drug target expression levels) and several interaction-based scores (based on randomly chosen partners, randomly chosen PPI partners of the drug target gene[s], the identified SL partners of other cancer drugs, and experimentally identified SL partners) in the three BRAF inhibitor cohorts (x axis).

(D) Bar graphs showing the fraction of responders in the patients with high SL-scores (top tertile; green) and low SL-scores (bottom tertile; purple). The gray line denotes the overall response rate in each cohort, and the stars denote the hypergeometric significance of enrichment of responders in the high-SL group and depletion of responders in the low-SL group (compared with their baseline frequency in the cohort).

(E and F) Kaplan-Meier curves depicting the survival of patients with low (yellow) versus high (blue) BRAF SL-scores (top versus bottom tertile of SL-scores) of (E) GSE50509 (Rizos et al., 2014) and (F) independent (unseen) BRAF inhibitor clinical trials (Wongchenko et al., 2017). Patients with high SL-scores show better prognosis, as expected. The log rank p value and median survival difference are denoted. See also Figures S2 and S3 and Tables S2 and S5.

procedures markedly reduce the well-known risk of obtaining overfitted predictors that would fail to predict on datasets other than those on which they were originally built.

SELECT prediction of response to targeted cancer therapies

We start by analyzing four melanoma cohorts treated with BRAF inhibitors for which pre-treatment transcriptomics data and response information are available (Hugo et al., 2015; Kakavand et al., 2017; Rizos et al., 2014). Applying SELECT, we identified the 25 most significant SL partners of BRAF (Table S2), where the number 25 was determined from training on one single dataset and kept fixed thereafter in all targeted therapy predictions (see STAR Methods for the details of parameter choices; Figures S1 and S2). As expected, we find that responders have higher SL-scores than non-responders in the three melanoma-BRAF cohorts for which therapy response data are available (Figure 2A). Quantifying the predictive power via the use of the standard area under the receiver operating characteristics curve (area under the curve [AUC] of the ROC curve) measure, we find AUCs greater than 0.7 in all three datasets and an aggregate performance of AUC = 0.71 when the three cohorts are merged (Figure 2B). As some datasets do not have a balanced number of responders and non-responders, we additionally quantified the resulting performance via precision-recall curves (often used as supplement to the routinely used ROC curves; Figure S3A). As evident from the latter, one can choose a single classification threshold that successfully captures most true responders while misclassifying less than half of the non-responders. Even though all patients in these three cohorts have either a BRAF V600E or V600K mutation, there is still a large variability in their response. SELECT successfully captures some of this variability to predict the patients who will respond better to BRAF inhibition.

Reassuringly, the SL-based prediction accuracy levels are overall higher compared with those obtained by several published transcriptomic-based predictors, including the proliferation index (Whitfield et al., 2006), interferon-γ (IFNγ) signature (Ayers et al., 2017), cytolytic score (Rooney et al., 2015), or the

Please cite this article in press as: Lee et al., Synthetic lethality-mediated precision oncology via the tumor transcriptome, Cell (2021), https://doi.org/10.1016/j.cell.2021.03.030

expression of the drug target gene itself (BRAF in this case). SL-based prediction accuracy levels are also better than other interaction-based scores, including the fraction of downregulated randomly selected genes, the fraction of *in vitro* experimentally determined SL partners (i.e., genes that pass the first step of Figure 1A), the fraction of the inferred SL partners of other drugs, or the fraction of downregulated protein-protein interaction (PPI) partners of drug targets (all of sizes similar to the SL set; empirical $p < 0.001$) (Figure 2C). Although studies have reported that V600E patients have a better response to vemurafenib than V600K patients (Pires da Silva et al., 2019), this has not been observed in the three melanoma cohorts that we analyzed, where the BRAF 600E mutant patients are not significantly enriched in responders. The BRAF SL-score and the BRAF mutation status are not significantly correlated, demonstrating that SL-score is not a mere readout of BRAF oncogenic mutation states (Figure S3B). The patients with high SL-score (defined as those in the top tertile) show significantly higher rate of response than the overall response rate, and the patients with low SL-score (in the bottom tertile) show the opposite trend (Figure 2D). We observe that patients with higher SL-scores showed significantly better treatment outcome in terms of progression-free survival (PFS) in the dataset mentioned above where these data were available to us (Figure 2E); the integrated analysis of large-scale BRAF inhibitor clinical trials (Wongchenko et al., 2017) ($n = 621$) also shows that the SL-score is associated with significantly improved PFS (Figure 2F). As expected, the SL partners of BRAF were found to be enriched with the functional annotation "regulation of GTPase-mediated signal transduction" (Fisher's exact test, $p < 0.002$).

We next test the prediction accuracy of the SL-based approach on a variety of targeted therapies and cancer types. We collected 23 additional publicly available datasets from clinical trials of cytotoxic agents and targeted cancer therapies, each one containing both pre-treatment transcriptomics data and therapy response information. This compendium includes breast cancer patients treated with lapatinib (Guarneri et al., 2015), tamoxifen (Desmedt et al., 2009), or gemcitabine (Julka et al., 2008); colorectal cancer patients treated with irinotecan (Graudens et al., 2006); multiple myeloma patients treated with bortezomib (Terragna et al., 2016) or dexamethasone (Manojlovic et al., 2017); acute myeloid leukemia patients treated with gemtuzumab (Bolouri et al., 2018); and hepatocellular carcinoma patients treated with sorafenib (Pinyol et al., 2019). In each dataset, we first identified the SL interaction partners of the targets of the drug given in that trial (STAR Methods; Table S2), and based on those, we computed the SL-score of each sample from its transcriptomics.

We first note that SELECT mostly fails in predicting the response to cytotoxic agents, obtaining AUC > 0.7 in only 2 of 11 of these datasets where RECIST information was available. This is not surprising given that the SL approach relies on the specificity and correct identification of the targets of each drug, and cytotoxic agents typically have a multitude of targets that are often poorly defined. This is in difference from the more recently developed targeted and immune checkpoint therapies that have better-defined targets. Indeed, we find that higher SL-scores are associated with better response in 4 of 7 targeted therapy datasets we could test. The results for the therapies that are successfully predicted (all AUCs > 0.7) are presented in Figures 3A and 3B, and the pertaining precision-recall curves are shown in Figure S3C. The predictive performance of a variety of expression-based control predictors is random (Figure 3C). Patients with high SL-scores (within top tertile) have significantly higher response rates than the overall response rates, and the patients with low SL-scores (within bottom tertile) show the opposite trend (Figure S3D). Importantly, in the four datasets where we have survival information, we observe that patients with higher SL-scores also have improved overall survival (Figures 3D–3G).

SELECT prediction of response to immune checkpoint blockade

We next turn to study the ability of SELECT to predict clinical response to immune checkpoint blockade. To identify the SR interaction partners that are predictive of the response to anti-PD1/PDL1 and anti-CTLA4 therapy, we introduced a few modifications in the published pipelines (Lee et al., 2018; Sahu et al., 2019), considering the characteristics of immune checkpoint therapy (STAR Methods). For anti-PD1/PDL1 therapy, where the antibody blocks the physical interaction between PD1 and PDL1, we considered the interaction term (i.e., the product of *PD1* and *PDL1* gene expression values) in identifying the SR partners of the treatment (STAR Methods). For anti-CTLA4 therapy, where the precise mechanism of action involves several ligand/receptor interactions (Wei et al., 2017), we focused on the CTLA4 itself, using its protein expression levels as they are likely to better reflect the activity than the mRNA levels. Using this immune-tailored version of SELECT, we analyzed the TCGA data to identify the SL and SR partners of PD1/PDL1 and of CTLA4. We could not identify statistically significant SL interaction partners of these checkpoint targets, but did identify significant pan-cancer SR interactions. In the latter, the inactivation of the target gene of a drug is compensated by the downregulation of another gene (termed the partner rescuer gene). Given an immune checkpoint drug and pre-treatment tumor transcriptomics data from a patient, we quantify the fraction f of SR partners that are downregulated in the tumor. We define $1-f$ as its SR-score, where tumors with higher SR-scores have less "active" rescuers and are hence expected to respond better to the therapy (STAR Methods).

To evaluate the accuracy of SR-based predictions, we collected a set of 21 immune checkpoint therapy datasets that included both pre-treatment transcriptomics data and therapy response information (either by RECIST or patient survival), overall comprised of 1,021 patients (Table S1). These datasets include melanoma (Chen et al., 2016; Gide et al., 2018; Huang et al., 2019; Liu et al., 2019; Nathanson et al., 2017; Prat et al., 2017; Van Allen et al., 2015), non-small cell lung cancer (Cho et al., 2020; Damotte et al., 2019; Hwang et al., 2020; Thompson et al., 2020), renal cell carcinoma (Braun et al., 2020; Miao et al., 2018), metastatic gastric cancer (Kim et al., 2018), and urothelial carcinoma (Snyder et al., 2017) cohorts treated with anti-PD1/PDL1, anti-CTLA4, or their combination. Indeed, we find that overall higher SR-scores are associated with better response to immune checkpoint blockade (Figure 4A), with AUCs > 0.7

Please cite this article in press as: Lee et al., Synthetic lethality-mediated precision oncology via the tumor transcriptome, Cell (2021), https://doi.org/10.1016/j.cell.2021.03.030

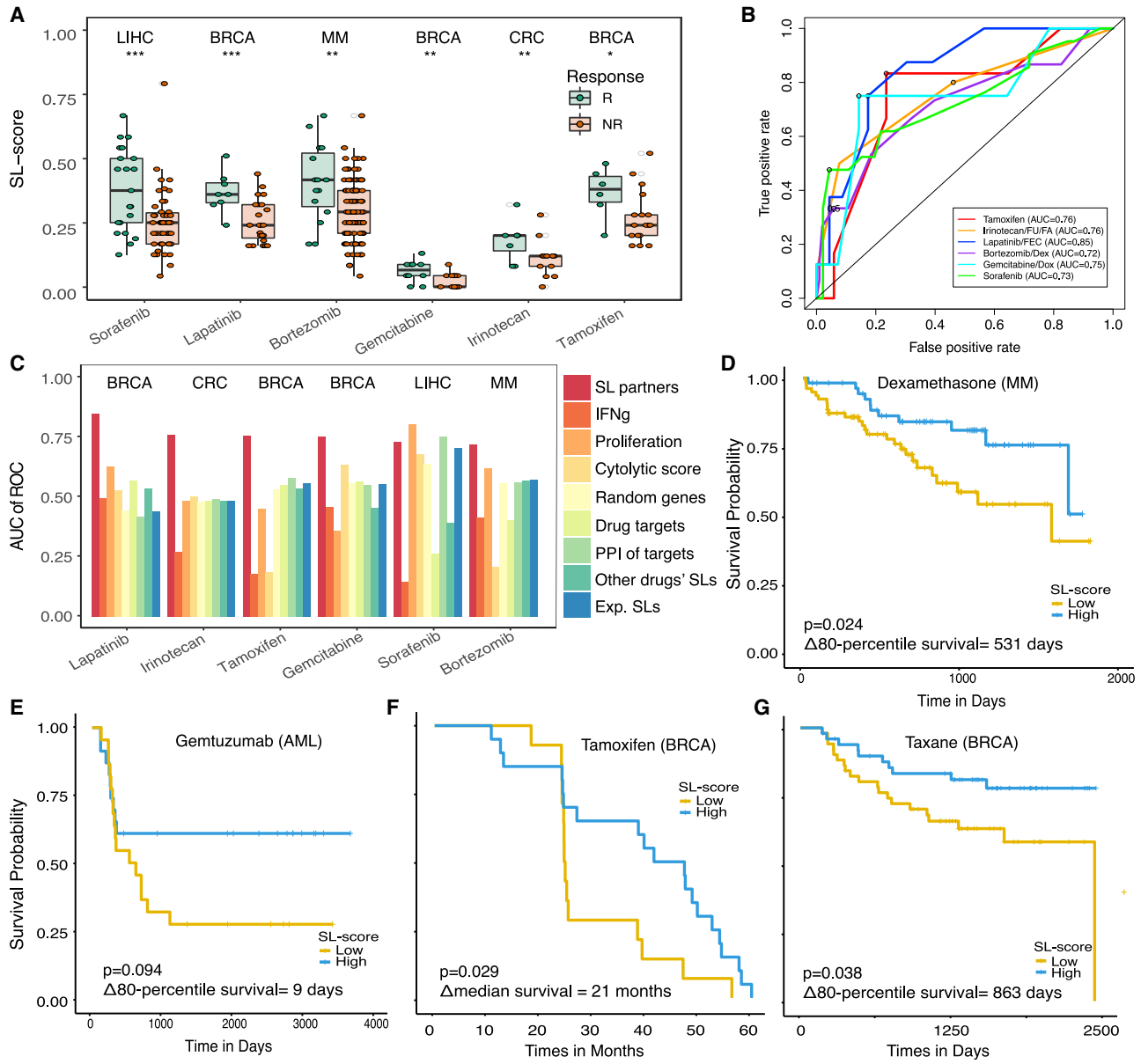

Figure 3. SELECT stratifies patients for targeted therapies across different cancer types

(A) SL-scores are significantly higher in responders (green) versus non-responders (red) based on Wilcoxon rank-sum test after multiple hypothesis correction. For false discovery rates, * denotes 10%, ** denotes 5%, and *** denotes 1%. Cancer types are noted on the top of each dataset.

(B) ROC curves for breast cancer patients treated with lapatinib (GSE66399) (Guarneri et al., 2015), tamoxifen (GSE16391) (Desmedt et al., 2009), or gemcitabine (GSE8465) (Julka et al., 2008); colorectal cancer patients treated with irinotecan (GSE3964) (Graudens et al., 2006); multiple myeloma patients treated with bortezomib (GSE68871) (Terragna et al., 2016); and hepatocellular carcinoma patients treated with sorafenib (GSE109211) (Pinyol et al., 2019). The circles denote the point of maximal F1-score.

(C) Bar graphs show the predictive accuracy in terms of AUCs (y axis) of SL-based predictors and a variety of controls specified earlier in Figure 2C (x axis).

(D–G) Kaplan-Meier curves depicting the survival of patients with low versus high SL-scores of (D) multiple myeloma patients treated with dexamethasone (Manojlovic et al., 2017) and (E) acute myeloid leukemia patients treated with gemtuzumab (Bolouri et al., 2018), (F) breast cancer patients treated with tamoxifen (GSE16391) (Desmedt et al., 2009), and (G) breast cancer patientss treated with taxane-anthracycline (GSE32603) (Magbanua et al., 2015), where x axis denotes survival time and y axis denotes the probability of survival. Patients with high SL-scores (top tertile, blue) show better prognosis than the patients with low SL-scores (bottom tertile, yellow), as expected. The log rank p values and median survival differences (or 80th percentile survival differences if survival exceeds 50% at the longest time point) are denoted in the figure. Tumor type abbreviations are as follows: MM, multiple myeloma; CRC, colorectal cancer; BRCA, breast invasive carcinoma; AML, acute myeloid leukemia; and LIHC, liver hepatocellular carcinoma. See also Figure S3 and Tables S2 and S5.

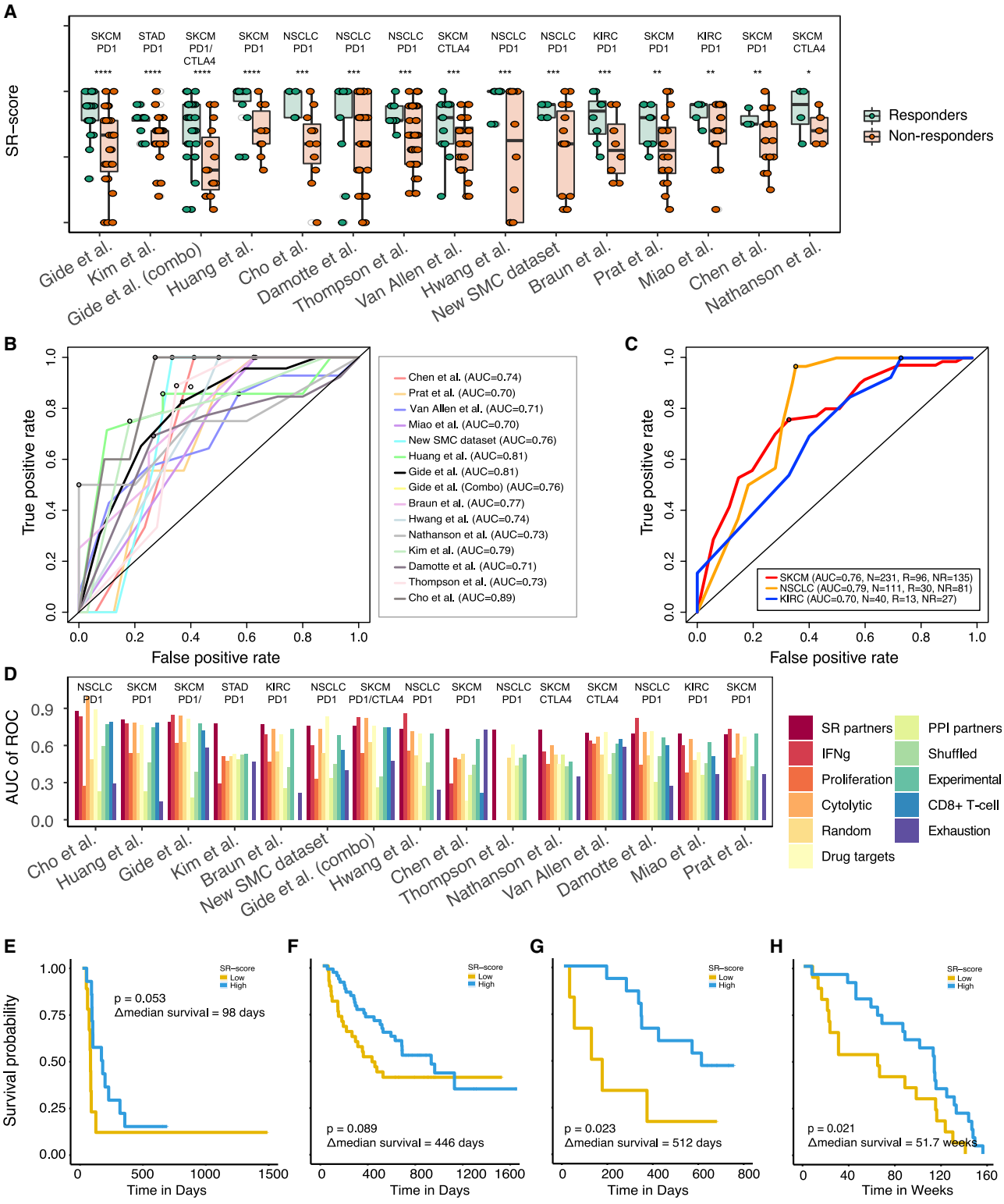

Figure 4. SELECT stratifies patients for immune checkpoint therapy across different cancer types

(A) SR-scores are significantly higher in responders (green) versus non-responders (red) based on Wilcoxon rank-sum test after multiple hypothesis correction. For false discovery rates, * denotes 20%, ** denotes 10%, *** denotes 5%, and **** denotes 1%. Cancer types are noted on the top of each dataset. Results are shown for melanoma (Chen et al., 2016; Gide et al., 2018; Liu et al., 2019; Nathanson et al., 2017; Prat et al., 2017; Van Allen et al., 2015), non-small cell lung cancer

(legend continued on next page)

Please cite this article in press as: Lee et al., Synthetic lethality-mediated precision oncology via the tumor transcriptome, Cell (2021), https://doi.org/10.1016/j.cell.2021.03.030

in 15 of 18 datasets where RECIST information is available (Figure 4B; for corresponding precision-recall curves, see Figure S3E). Notably, SELECT remains predictive when multiple datasets of the same cancer types are combined for melanoma, non-small cell lung cancer, or kidney cancer (Figure 4C).

The prediction accuracy of SELECT is overall superior to a variety of expression-based controls (Figure 4D) including T cell exhaustion markers (Wherry et al., 2007) and the estimated $CD8^+$ T cell abundance (Newman et al., 2015). Notably, SELECT is also predictive for a new unpublished dataset of lung adenocarcinoma patients treated with pembrolizumab, an anti-PD1 checkpoint inhibitor, at Samsung Medical Center (SMC) (STAR Methods; Figures 4A, 4B, and 4D [denoted as "new SMC dataset"]). As expected, patients with high SR-scores (in the top tertile) are enriched with responders, while patients with low SR-scores (in the bottom tertile) are enriched with non-responders (Figure S3F). We also analyzed three recently published anti-PD1 glioblastoma trials (Cloughesy et al., 2019; Schalper et al., 2019; Zhao et al., 2019), where even though their overall efficacy was moderate, the SR-score shows a considerable predictive signal (Figures S3G and S3H). Finally, the SR-scores are also predictive of progression-free or overall patient survival in four different checkpoint inhibition cohorts where these data was available (Figures 4E–4H).

The predicted SR partners of PD1/PDL1 and CTLA4 (Figure 5A) are enriched for T cell apoptosis and response to inlerlueikn-15 (IL-15) pathways (Figure S3I). They include key immune genes such as *CD4*, *CD8A*, and *CD274*, and PPI partners of PD1/PDL1 and CTLA4 such as *CD44*, *CD27*, and *TNFRSF13B*. The contribution of individual SR partners to the response prediction is different across different datasets from different cancer types (Figure 5B), where *CD4*, *CD27*, and *CD8A* play an important role in many samples. Taken together, these results testify that the SR partners of PD1/PDL1 and CTLA4 serve as effective biomarkers for checkpoint response across a wide range of cancer types.

To study whether tumor-specific SR-scores can explain the variability observed in the objective response rates (ORRs) of different tumor types to immune checkpoint therapy, we computed the SR-scores for anti-PD1 therapy for each tumor sample in the TCGA (STAR Methods). Comparing these scores with the threshold SR-score for determining responders, we computed the fraction of predicted responders to anti-PD1 therapy in each cancer type in the TCGA cohort. We then compared these predicted cancer-specific fractions with the actual ORR observed in anti-PD1 clinical trials of 16 cancer types (Lee and Ruppin, 2019; Yarchoan et al., 2017). Notably, we find that these two measures significantly correlate (Figure 5C), demonstrating that SR-scores are effective predictors of ORR to checkpoint therapy across different cancer types.

Summing up over the three classes of the drugs that we studied, SELECT achieves greater than 0.7 AUC predictive performance levels in 24 of 39 datasets containing RECIST response information, spanning 2 of 11 non-targeted cytotoxic agents, 7 of 10 targeted therapies, and 15 of 18 immunotherapy cohorts (including our new SMC dataset) (Figure 6). Adding the 7 (of 9) additional datasets where SL/SR-score is predictive of progression-free or overall survival (1 chemotherapy, 3 targeted therapy, and 3 immunotherapy), it is predictive in 31 of 48 cohorts overall (65%) and in 28 of 35 (80%) cohorts among the targeted and checkpoint therapies. Notably, these accuracies are markedly better than those obtained using a range of control predictors.

A retrospective analysis of the WINTHER trial

To evaluate SELECT in a multi-arm basket clinical trial setting, we performed a retrospective analysis of the recent WINTHER trial data, the first large-scale basket prospective clinical trial that has incorporated transcriptomics data for cancer therapy in adult patients with advanced solid tumors (Rodon et al., 2019). This multi-center study had two arms: one recommending treatment based on actionable mutations in a panel of cancer driver genes and the other based on the patients' transcriptomics data. We considered the gene expression data of 71 patients with 50 different targeted treatments (single or combinations) for which significant SL partners were identified. One patient had a complete response, 7 had a partial response, and 11 were reported to have stable disease (labeled as responders), while 52 had progressive disease (labeled as non-responders).

We first applied SELECT to identify the SL partners for each of the drugs prescribed in the study (STAR Methods). The resulting SL-scores of the therapies used in the trial are significantly higher in responders than non-responders (Wilcoxon rank-sum $p < 0.05$; Figure 7A). Notably, the SL-scores of the drugs given to each patient are predictive of the actual responses observed in the trial (AUC = 0.72 [Figure 7B], with an SL-score of 0.44 chosen as optimal threshold with maximal F1-score [Figures S4A and S4B]). As shown in Figure 7C, the prediction accuracy of SL-score is superior to that of control expression-based predictors. This reassuring predictive signal led us to evaluate how many patients are predicted to benefit from the set of drugs used in the

(Cho et al., 2020; Damotte et al., 2019; Hwang et al., 2020; Thompson et al., 2020), renal cell carcinoma (Braun et al., 2020; Miao et al., 2018), and metastatic gastric cancer (Kim et al., 2018) treated with anti-PD1/PDL1, anti-CTLA4, or their combination and our new lung adenocarcinoma cohort treated with anti-PD1 (GEO: GSE166449).

(B and C) ROC curves showing the prediction accuracy obtained with the SELECT framework (B) in the 15 different datasets and (C) across their cancer-type-specific aggregation in melanoma, non-small cell lung cancer, and kidney cancer. The circles denote the point of maximal F1-score.

(D) Bar graphs show the predictive accuracy in terms of AUC (y axis) of SR-based predictors and controls across the 15 different cohorts (x axis) (control predictors are similar to those described in Figure 2C, with the addition of T cell exhaustion and $CD8^+$ T cell abundance).

(E–H) Kaplan-Meier curves depicting the survival of patients with low versus high SR-scores in (E) anti-PD1/CTLA4 combination-treated melanoma (Gide et al., 2018), (F) nivolumab/pembrolizumab-treated melanoma (Liu et al., 2019), (G) atezolizumab-treated urothelial cancer (Snyder et al., 2017), and (H) nivolumab-treated melanoma (Riaz et al., 2017) cohorts. Patients with high SR-scores (blue; over top tertile) show better prognosis than the patients with low SR-scores (yellow; below bottom tertile), and the log rank p values and median survival differences are denoted. Tumor type abbreviations are as follows: STAD, stomach adenocarcinoma, SKCM, skin cutaneous melanoma; NSCLC, non-small cell lung cancer; and KIRC, kidney renal clear cell carcinoma. See also Figure S3 and Table S4.

Please cite this article in press as: Lee et al., Synthetic lethality-mediated precision oncology via the tumor transcriptome, Cell (2021), https://doi.org/10.1016/j.cell.2021.03.030

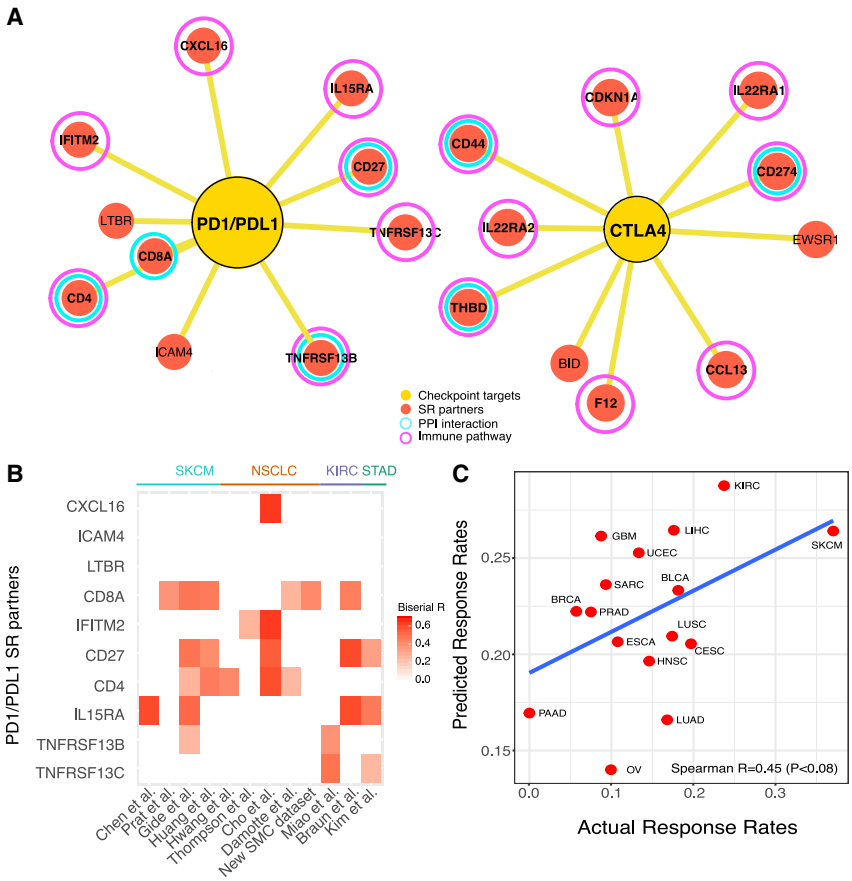

Figure 5. Meta-analysis of SELECT SR partners for immune checkpoint therapy

(A) The SR partners of PD1-PDL1 interaction (left) and CTLA4 (right), where red circles denote SR partners, yellow circles denote checkpoint targets, purple circles denote genes that belong to immune pathways, and cyan circles denote a protein-protein interaction (based on STRING database; Szklarczyk et al., 2015) with PD1/PDL1 or CTLA4, respectively.

(B) A heatmap showing the association of individual SR partners' gene expression (y axis) with anti-PD1/PDL1 response in the 12 clinical trial cohorts (x axis). The significant point-biserial correlation coefficients are color coded ($p < 0.1$), and the cancer types of each cohort are denoted on the top of the heatmap.

(C) The SR-based predicted response rates for different TCGA cancer types (y axis) correlate with the objective response rates observed in independent clinical trials across these cancer types (x axis) (Spearman R = 0.45, $p < 0.08$), with a regression line (blue). Tumor type abbreviations are as follows: UCEC, uterine corpus endometrial carcinoma; STAD, stomach adenocarcinoma, SKCM, skin cutaneous melanoma; SARC, sarcoma; PRAD, prostate adenocarcinoma; PAAD, pancreatic adenocarcinoma; OV, ovarian serous cystadenocarcinoma; NSCLC, non-small cell lung cancer; LUAD, lung adenocarcinoma; LUSC, lung squamous cell carcinoma; LIHC, liver hepatocellular carcinoma; KIRC, kidney renal clear cell carcinoma; HNSC, head-neck squamous cell carcinoma; GBM, glioblastoma multiforme; ESCA, esophageal carcinoma; CESC, cervical squamous cell carcinoma and endocervical adenocarcinoma; BRCA, breast invasive carcinoma; and BLCA, bladder carcinoma. See also Figure S3.

trial, if the treatment choices would have been guided by SELECT?

To answer this question in a systematic manner, we identified the top predicted drugs in every patient individually by computing the SL-scores of all cohort drugs based on the patients' tumor transcriptomics (STAR Methods). For approximately 94% (67/71) of the patients, we could identify therapies that have higher SL-scores than those of the drugs prescribed to them in the WINTHER trial (Figure 7D). Based on the 0.44 optimal classification threshold identified as mentioned above, we estimate that 65% (46/71) of the patients would respond to the new treatments (with 10% false positive rate), compared with 27% that responded (based on either targeted DNA sequencing or transcriptomics) in the original trial. Of the 52 non-responders reported in the original trial, we find that 62% (32/52) can be matched with predicted effective therapies (with 10% false positive rate) (Figure 7D; Figure S4C). We note that while this analysis focuses on SL-based treatment recommendations, obviously, other non-SL mechanisms may underlie patients' response to different drugs.

Notably, Figure 7D clearly shows a trend where patients in the WINTHER trial that were predicted to respond well to one of the drugs used in the trial were often predicted to respond to quite a few of these drugs. Following this observation, we considered the mean value of the SL-scores across all the drugs that were used in the WINTHER trial, which we term "mean SL-score" of a given sample. This score represents the tendency of a tumor to respond to any targeted therapy given in the cohort, a surrogate for its overall vulnerability. Notably, we find that SELECT is more predictive in the patient cohorts where the mean SL-score is high (computed over all the samples in a given cohort) than in those where it is low (Figure S5). This analysis indicates that SELECT works better in cohorts where the tumors are overall more vulnerable (as quantified by the mean SL-score). This is quite notable as it suggests that SELECT may actually offer more targeted treatment opportunities in more advanced tumors (with more genomic and transcriptional alterations).

To illustrate the potential future application of SELECT for patient stratification, we briefly describe here two individual cases arising in the WINTHER data analysis. The first involves a 75-year-old male patient with colon cancer who was treated with cabozantinib because of p53 and APC mutations, and the patient indeed responded to the therapy. SELECT also recommends the treatment of cabozantinib, bringing additional support to the treatment given (Figure 7E). The second example involves a 78-year-old female patient with lung cancer who was treated with nintedanib in the WINTHER trial because of KIF5B-RET fusion, but failed to respond to the therapy. SELECT

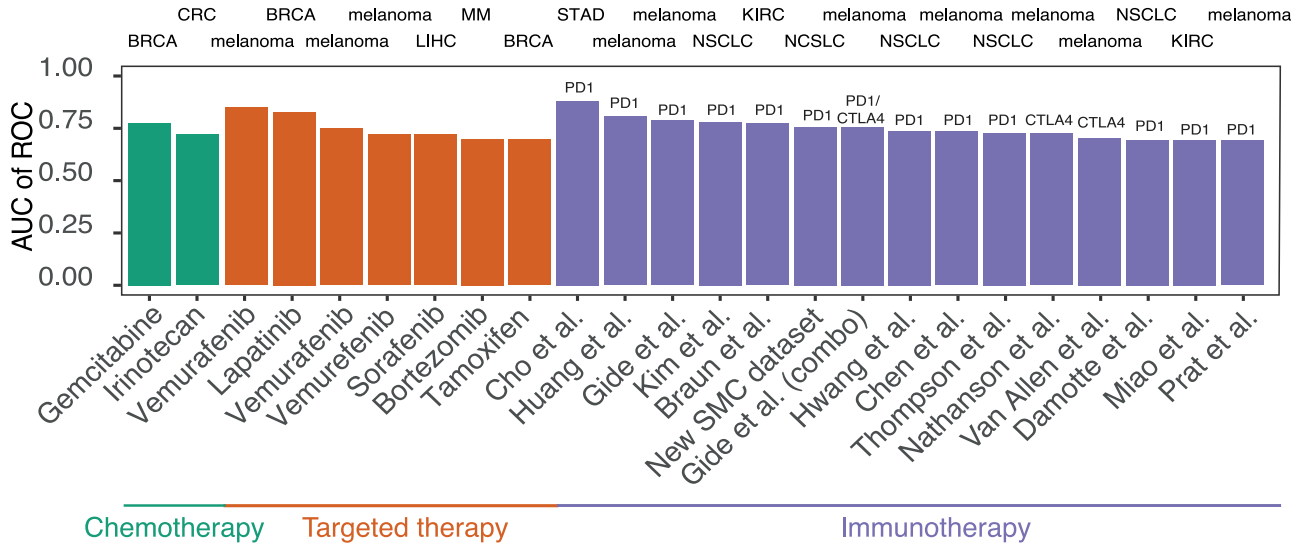

Figure 6. Overall prediction accuracy of SELECT precision oncology framework

The bar graphs show the overall predictive accuracy of SELECT for chemotherapy (red), targeted therapy (green), and immunotherapy (purple) in 24 different cohorts encompassing 8 different cancer types and 9 treatment options (for which discrete response information such as RECIST was given). Tumor type abbreviations are as follows: STAD, stomach adenocarcinoma; NSCLC, non-small cell lung cancer; MM, multiple myeloma; LIHC, liver hepatocellular carcinoma; KIRC, kidney renal clear cell carcinoma; CRC, colorectal cancer; BRCA, breast invasive carcinoma; and BLCA, bladder carcinoma.

assigns a low SL-score to nintedanib, but suggests an alternative treatment option, olaratumab, that obtains a much higher SL-score (Figure 7F). Overall, the drugs most frequently recommended by SELECT in this cohort are estramustine for their MAP1A/MAP2 inhibition followed by proteasome inhibitor (bortezomib) and MEK inhibitor (cobimetinib) (Figure 7G).

We further performed an SL-based drug coverage analysis in another independent transcriptomics-based trials dataset, from the TEMPUS cohort (Beaubier et al., 2019), focusing on the same cancer types and drugs as those studied in the WINTHER trial, shows a similar pattern of top recommended drugs (Figure 7H), pointing to the robustness of these predictions across a variety of patient cohorts. One of the top-predicted drugs in both cohorts is the MEK inhibitor cobimetinib (>6% coverage in both cohorts), which is recommended for melanoma and lung cancer patients and is now being clinically tested across different cancer types (Grimaldi et al., 2017). In addition to the WINTHER and TEMPUS cohorts, we analyzed the recently released POG570 cohort, where the post-treatment transcriptomics data together with treatment history are available for advanced or metastatic tumors of 570 patients (Pleasance et al., 2020). We first confirmed that SL-scores are associated with longer treatment duration, which served as a proxy for therapeutic response in the original publication (Figure S6A). We further confirmed that this trend holds true per individual cancer types (Figure S6B) and across individual drugs (Figure S6C).

Finally, we asked whether SELECT can successfully estimate the ORRs observed across different drug treatments in different clinical trials for a given cancer type. As these trials did measure and report the patients' tumor transcriptomics, we estimated the coverage of each drug (the patients who are predicted to respond based on their SL-scores being larger than the 0.44 response threshold) in the TCGA cohort of the relevant cancer type (STAR Methods). We collected ORR data from multiple clinical trials in melanoma and non-small cell lung cancer (a total of 3,246 patients from 18 trials) (Table S3). Reassuringly, we find that the resulting estimated coverage is significantly correlated with the observed ORR in each of these cancer types (Figure S7).

DISCUSSION

We have demonstrated that by mining large-scale "-omics" data from patients' tumors, one can computationally infer putative pairs of GIs that can be used as predictive biomarkers for a variety of targeted and immunotherapy treatments, across multiple cancer types. The resulting prediction accuracy is considerable for many of the drugs tested. Furthermore, as shown in the analysis of the WINTHER trial, its application offers a promising way to increase the number of patients that could benefit from precision-based treatments, which should be further explored in prospective studies.

SELECT is fundamentally different from previous efforts for therapy response prediction in two important ways: (1) The SL/SR interactions underlying the prediction are inferred from analyzing pre-treatment data from the TCGA ensemble; they are further filtered using very limited training on a single treatment response dataset to set up a small number of classification hyper-parameters. This approach results in predictors that are likely to be less prone to the risk of overfitting, which frequently accompanies contemporary supervised predictors that are constructed by training on the relatively small clinical datasets. Furthermore, the SL/SR interactions used in this study are shared across many different cancer types, making them less context sensitive and more likely to be predictive in different

Please cite this article in press as: Lee et al., Synthetic lethality-mediated precision oncology via the tumor transcriptome, Cell (2021), https://doi.org/10.1016/j.cell.2021.03.030

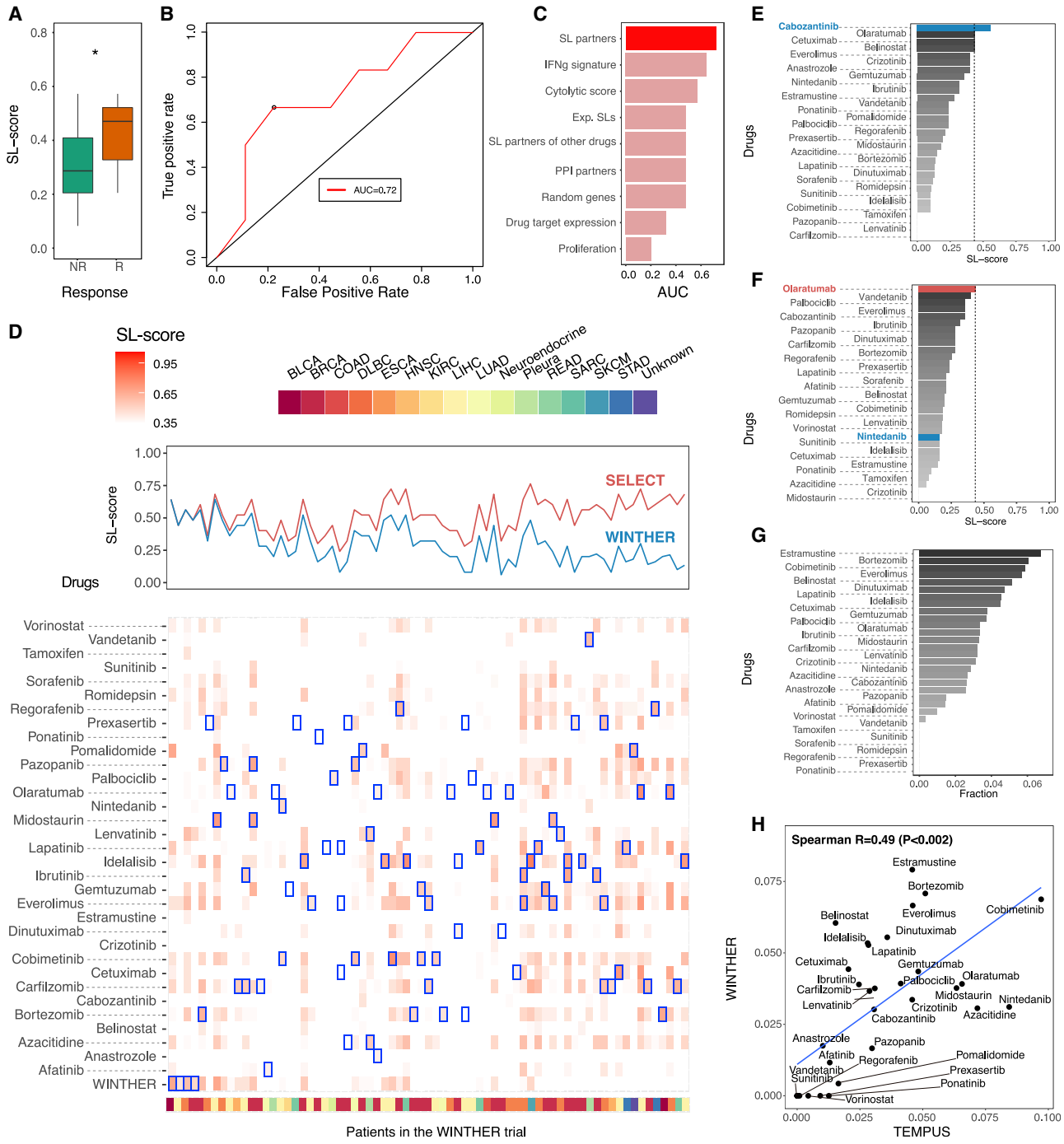

Figure 7. SELECT analysis of the WINTHER trial

(A) Responders (CR, PR, and SD; red) show significantly higher SL-scores compared with non-responders (PD; green) (Wilcoxon rank-sum $p < 0.05$).

(B) SL-scores are predictive of response to the different treatments prescribed at the trial (AUC of ROC = 0.72). The black circle denotes the point of maximal F1-score (corresponding to an SL-score threshold of 0.44).

(C) Bar graphs show the predictive accuracy in terms of AUC (x axis) of SL-based predictors and different controls (y axis) (control types are similar to those described in Figure 2C).

(D) (Top) Comparison of the SL-scores (y axis) of the treatments actually prescribed in the WINTHER trial (blue) and the SL-scores of the best therapy identified by our approach (red) across all 71 patients; samples are ordered by the difference in the two SL-scores. (Bottom) A more detailed display of the SL-scores of the treatment given in the trial (bottom row) and of all candidate therapies (all other rows), for all 71 patients (the treatments considered are denoted in every column). Blue boxes denote the highest SL-scoring treatments predicted for each patient. Cancer types of each sample are color coded at the bottom of the figure.

(legend continued on next page)

Please cite this article in press as: Lee et al., Synthetic lethality-mediated precision oncology via the tumor transcriptome, Cell (2021), https://doi.org/10.1016/j.cell.2021.03.030

cancer types. (2) Notably, the interactions enabling the predictions have clear biological meanings, as the functional interpretation of the arising SL/SR interactions and their scoring are simple and intuitive, differing from the typical "black-box" solutions characteristic of machine learning approaches.

The predictive performance of SELECT is superior to existing predictors. As far as we are aware, no single model has previously been shown to obtain such predictive accuracies across so many targeted and immunotherapy datasets. Reassuringly, while many of the currently available immune checkpoint cohorts are small, SELECT maintains its prediction accuracy when multiple cohorts are merged. The aggregate AUCs for melanoma, non-small cell lung cancer, and renal cell carcinoma (where multiple cohorts are available) are also greater than 0.7. This suggests SL/SR-scores in multiple datasets in a given cancer type have a similar distribution (see Figure 4A compared with Figure 3A), enabling the use of a single uniform threshold, testifying to its generalizability. In computing the SL/SR-score, we considered the fraction of "down"regulated partners rather than "up"regulated partners. This is because it is less noisy to determine cases where a gene is under-expressed than over-expressed, since overexpression could result from a number of different factors, including the expression arising from a multitude of different cell types that are present in the tumor microenvironment.

SELECT opens a possibility for future prospective clinical studies based on tumor transcriptomics. For such prospective clinical trials, we suggest that initially a more conservative predictive threshold may be used, recommending treatments only where the SL/SR predictions have a very strong and clear support. Additionally, one should obviously be careful not to use SELECT as evidence for precluding other promising treatment options that may arise due to non-SL/SR tumor vulnerabilities. The SELECT stratification signatures of each drug are focused on a small number of genes, suggesting that gene expression panels could be designed and readily incorporated in future trials in a cost-effective manner. Applying SELECT in the clinic would require overcoming two logistic challenges: (1) the need to obtain the genomics data and provide the analysis report in a timely manner and (2) the need to address the noisy nature of the transcriptomics data, via careful standardization and normalization. Reassuringly, most of the transcriptomics data we analyzed in this study are from formalin-fixed paraffin-embedded (FFPE) samples, which are the ones most commonly used in clinical practice. Notably, we are not relying on absolute expression values, but rather on the genes' relative ranking in the cohort, decreasing the sensitivity of our approach to potential transcriptomic measurement noise.

Importantly, we anticipate that the predictive performance of SELECT could be further improved in the foreseeable future. Such efforts will leverage on the increasing availability of accumulating tumor proteomic data and the development of computational approaches for inferring GIs from single-cell sequencing data or cell-type-specific expression levels derived from deconvolving bulk RNA-seq data, which will clarify the contribution of tumor heterogeneity and tumor microenvironment. Of note, the latter will enable the identification of GIs that are grounded on specific cell types (e.g., between tumor cells and $CD8^+$ T cell in their environment). As more data accumulate, we may learn how to combine SL and SR interactions together to further boost prediction performance.

In summary, this work introduces the first systematic transcriptomics-based precision oncology framework: SELECT. This framework prioritizes effective therapeutic options for cancer patients based on the biologically grounded concept of GIs, which are validated on an unprecedented scale across many different treatments and cancer types. Our study provides both explicit stratification signatures and a computational pipeline, freely available for academic use, which lay a basis for further testing and improvement in future transcriptomics-based precision oncology clinical trials.

Limitations of study

Like other genome-wide computational prediction method, SELECT has several limitations that should be acknowledged and improved upon in the future. (1) The large-scale screens and patient tumor data that are used for inferring the SL and SR interactions are obviously noisy, both on the molecular and on the phenotypic side. Given these data limitations, we took a conservative approach that is focused on inferring common core of "pan-cancer" interactions that are shared across different tumor types, while obviously there are important cancer-type-specific (and even sub-type) interactions that should be inferred in the future, as more data accumulate. (2) SELECT works by inferring the SL/SR interactions of the targets of the drugs. To this end, it uses the currently best-established mappings of these targets, but those are noisy and imperfect, too (and this may be one likely reason why SELECT performs poorly on chemotherapy drugs). Furthermore, while the mechanism of action of most cancer drugs does involve the inhibition of their targets, it is not the case for a few important cancer drugs, precluding the use of SELECT for such drugs; one such notable example is PARP inhibitors, whose mechanism of action results in the binding the PARP protein to the DNA, causing DNA-damage-induced cell death (furthermore, there is no PARP clinical trial data available with transcriptomics on which we could potentially test SL-based predictors, should one be able to infer them). (3) Last, but possibly the most important limitation that should be stated, is that while SELECT has been retrospectively tested in a large collection of anti-cancer clinical trials, future prospective clinical trials are needed to carefully assess and further improve its potential translational benefits.

(E and F) SELECT recommendations for two individual patients in the WINTHER trial. The x axis denotes the SL-score, and the y axis lists the different cohort treatments. The drugs given in WINTHER trial are colored in blue, and the top prediction by SELECT is in red.
(G) A bar graph showing the frequency (x axis) of the drugs (y axis) predicted to be most effective across the WINTHER cohort.
(H) The correlation between the estimated coverage of top-predicted drugs in the WINTHER cohort (y axis) and in a TEMPUS cohort of corresponding cancer types (n = 98). See also Figures S4, S5, S6, S7, and Table S5.

STAR★METHODS

Detailed methods are provided in the online version of this paper and include the following:

- KEY RESOURCES TABLE
- RESOURCE AVAILABILITY
  - Lead contact
  - Materials availability
  - Data and code availability
- METHOD DETAILS
  - Data collection
  - The SELECT pipeline
  - Samsung Medical Center anti-PD1-treated lung adenocarcinoma cohort
  - TCGA anti-PD1 coverage analysis for predicting the cancer type-specific response to checkpoint therapy
  - Retrospective analysis of the WINTHER trial
  - Coverage analysis on TCGA data for melanoma and non-small-cell lung cancer
- QUANTIFICATION AND STATISTICAL ANALYSIS
- ADDITIONAL RESOURCES

SUPPLEMENTAL INFORMATION

Supplemental information can be found online at https://doi.org/10.1016/j.cell.2021.03.030.

ACKNOWLEDGMENTS

This research is supported in part by the Intramural Research Program of the National Institutes of Health (NIH), National Cancer Institute (NCI), Center for Cancer Research (CCR). This work utilized the computational resources of the NIH HPC Biowulf cluster. We thank E. Michael Gertz, Alejandro A. Schäffer, Sanna Madan, Peng Jiang, Tom Misteli, and Louis Staudt for providing many helpful comments. We thank all the patients and clinicians involved in the clinical trials analyzed in this study. We thank Elizabeth Jaffe, Ignacio Melero, Robert Prins, Raul Rabadan, Antoni Ribas, Jeffrey Thompson, Nitin Roper, and Udayan Guha for sharing their data. This publication is partly based on research using data from Tempus Labs that has been made available through Vivli. Vivli has not contributed to or approved of and is not in any way responsible for the contents of this publication. J.S.L. is partly supported by a grant of the National Research Foundation of Korea funded by the Korean Government (NRF-2020R1A2C2007652) and Institute of Information & Communications Technology Planning & Evaluation (IITP) grant funded by the Korean Government (MSIT) (no. 2019-0-00421, AI Graduate School Support Program [Sungkyunkwan University]).

AUTHOR CONTRIBUTIONS

J.S.L. and E.R. led the study and J.S.L., K.A., and E.R. wrote the manuscript. N.U.N. and G.D. helped with the computational analysis. L.C., S.S., K.W., H.C., A.V.S., S.H., E.R., V.L., R.B., A.S., and S.-H.L. helped with data collection. N.U.N., G.D., D.K., and Y.C. helped reviewing the source code. N.U.N., G.D., T.B., Z.R., S.H., M.R.G., R.K., and K.A. contributed to the conceptual construction of the study.

DECLARATION OF INTERESTS

E.R. is a co-founder of Medaware, Metabomed, and Pangea Therapeutics (divested from the latter). E.R. serves as a non-paid scientific consultant to Pangea Therapeutics, a company developing a precision oncology SL-based multi-omics approach. J.S.L. is a scientific consultant; T.B. is chief executive officer and chief technical officer; G.D. is head of research and development; R.B. is a member of the Scientific Advisory Board; and Z.R. is a co-founder and a scientific advisor at Pangea Therapeutics. R.K. receives research funding from Genentech, Merck Serono, Pfizer, Boehringer Ingelheim, TopAlliance, Takeda, Incyte, Debiopharm, Medimmune, Sequenom, Foundation Medicine, Konica Minolta, Grifols, Omniseq, and Guardant; received consultant, speaker, and/or advisory board fees for X-Biotech, Neomed, Pfizer, Actuate Therapeutics, Roche, Turning Point Therapeutics, TD2/Volastra, and Bicara Therapeutics; has an equity interest in IDbyDNA and CureMatch; serves on the board of CureMatch and CureMetrix; and is a co-founder of CureMatch. A patent application associated with this manuscript is in process.

Received: April 14, 2020
Revised: October 29, 2020
Accepted: March 12, 2021
Published: April 12, 2021

REFERENCES

Aguirre, A.J., Meyers, R.M., Weir, B.A., Vazquez, F., Zhang, C.Z., Ben-David, U., Cook, A., Ha, G., Harrington, W.F., Doshi, M.B., et al. (2016). Genomic Copy Number Dictates a Gene-Independent Cell Response to CRISPR/Cas9 Targeting. Cancer Discov. *6*, 914–929.

Antonia, S.J., Villegas, A., Daniel, D., Vicente, D., Murakami, S., Hui, R., Yokoi, T., Chiappori, A., Lee, K.H., de Wit, M., et al. (2017). Durvalumab after chemoradiotherapy in stage III non–small-cell lung cancer. New England Journal of Medicine *377*, 1919–1929.

Ayers, M., Lunceford, J., Nebozhyn, M., Murphy, E., Loboda, A., Kaufman, D.R., Albright, A., Cheng, J.D., Kang, S.P., Shankaran, V., et al. (2017). IFN-γ-related mRNA profile predicts clinical response to PD-1 blockade. J. Clin. Invest. *127*, 2930–2940.

Barretina, J., Caponigro, G., Stransky, N., Venkatesan, K., Margolin, A.A., Kim, S., Wilson, C.J., Lehár, J., Kryukov, G.V., Sonkin, D., et al. (2012). The Cancer Cell Line Encyclopedia enables predictive modelling of anticancer drug sensitivity. Nature *483*, 603–607.

Basu, A., Bodycombe, N.E., Cheah, J.H., Price, E.V., Liu, K., Schaefer, G.I., Ebright, R.Y., Stewart, M.L., Ito, D., Wang, S., et al. (2013). An interactive resource to identify cancer genetic and lineage dependencies targeted by small molecules. Cell *154*, 1151–1161.

Beaubier, N., Bontrager, M., Huether, R., Igartua, C., Lau, D., Tell, R., Bobe, A.M., Bush, S., Chang, A.L., Hoskinson, D.C., et al. (2019). Integrated genomic profiling expands clinical options for patients with cancer. Nat. Biotechnol. *37*, 1351–1360.

Bolouri, H., Farrar, J.E., Triche, T., Jr., Ries, R.E., Lim, E.L., Alonzo, T.A., Ma, Y., Moore, R., Mungall, A.J., Marra, M.A., et al. (2018). The molecular landscape of pediatric acute myeloid leukemia reveals recurrent structural alterations and age-specific mutational interactions. Nat. Med. *24*, 103–112.

Brahmer, J., Reckamp, K.L., Baas, P., Crinò, L., Eberhardt, W.E.E., Poddubskaya, E., Antonia, S., Pluzanski, A., Vokes, E.E., Holgado, E., et al. (2015). Nivolumab versus docetaxel in advanced squamous-cell non–small-cell lung cancer. New England Journal of Medicine *373*, 123–135.

Braun, D.A., Hou, Y., Bakouny, Z., Ficial, M., Sant' Angelo, M., Forman, J., Ross-Macdonald, P., Berger, A.C., Jegede, O.A., Elagina, L., et al. (2020). Interplay of somatic alterations and immune infiltration modulates response to PD-1 blockade in advanced clear cell renal cell carcinoma. Nat. Med. *26*, 909–918.

Cancer Genome Atlas Research Network, Weinstein, J.N., Collisson, E.A., Mills, G.B., Shaw, K.R., Ozenberger, B.A., Ellrott, K., Shmulevich, I., Sander, C., and Stuart, J.M. (2013). The Cancer Genome Atlas Pan-Cancer analysis project. Nat. Genet. *45*, 1113–1120.

Chen, P.L., Roh, W., Reuben, A., Cooper, Z.A., Spencer, C.N., Prieto, P.A., Miller, J.P., Bassett, R.L., Gopalakrishnan, V., Wani, K., et al. (2016). Analysis of Immune Signatures in Longitudinal Tumor Samples Yields Insight into Biomarkers of Response and Mechanisms of Resistance to Immune Checkpoint Blockade. Cancer Discov. *6*, 827–837.

Cheung, H.W., Cowley, G.S., Weir, B.A., Boehm, J.S., Rusin, S., Scott, J.A., East, A., Ali, L.D., Lizotte, P.H., Wong, T.C., et al. (2011). Systematic investigation of genetic vulnerabilities across cancer cell lines reveals lineage-specific dependencies in ovarian cancer. Proc. Natl. Acad. Sci. USA *108*, 12372–12377.

Cho, J.W., Hong, M.H., Ha, S.J., Kim, Y.J., Cho, B.C., Lee, I., and Kim, H.R. (2020). Genome-wide identification of differentially methylated promoters and enhancers associated with response to anti-PD-1 therapy in non-small cell lung cancer. Exp. Mol. Med. *52*, 1550–1563.

Cloughesy, T.F., Mochizuki, A.Y., Orpilla, J.R., Hugo, W., Lee, A.H., Davidson, T.B., Wang, A.C., Ellingson, B.M., Rytlewski, J.A., Sanders, C.M., et al. (2019). Neoadjuvant anti-PD-1 immunotherapy promotes a survival benefit with intratumoral and systemic immune responses in recurrent glioblastoma. Nat. Med. *25*, 477–486.

Cowley, G.S., Weir, B.A., Vazquez, F., Tamayo, P., Scott, J.A., Rusin, S., East-Seletsky, A., Ali, L.D., Gerath, W.F., Pantel, S.E., et al. (2014). Parallel genome-scale loss of function screens in 216 cancer cell lines for the identification of context-specific genetic dependencies. Sci. Data *1*, 140035.

Damotte, D., Warren, S., Arrondeau, J., Boudou-Rouquette, P., Mansuet-Lupo, A., Biton, J., Ouakrim, H., Alifano, M., Gervais, C., Bellesoeur, A., et al. (2019). The tumor inflammation signature (TIS) is associated with anti-PD-1 treatment benefit in the CERTIM pan-cancer cohort. J. Transl. Med. *17*, 357.

Daud, A., Kluger, H.M., Kurzrock, R., Schimmoller, F., Weitzman, A.L., Samuel, T.A., Moussa, A.H., Gordon, M.S., and Shapiro, G.I. (2017). Phase II randomised discontinuation trial of the MET/VEGF receptor inhibitor cabozantinib in metastatic melanoma. British journal of cancer *116* (4), 432–440.

Decoster, L., Neyns, B., Vande Broek, I., Anckaert, E., De Clerck, D., DeMajois, MeyF.J., Baurain, J., Denys, H., and De Greve, J. (2010). Activity of sunitinib in advanced malignant melanoma and its correlation with potential predictive biomarkers. Journal of Clinical Oncology *28*, 8518–8518.

Del Rio, M., Mollevi, C., Bibeau, F., Vie, N., Selves, J., Emile, J.F., Roger, P., Gongora, C., Robert, J., Tubiana-Mathieu, N., et al. (2017). Molecular subtypes of metastatic colorectal cancer are associated with patient response to irinotecan-based therapies. Eur. J. Cancer *76*, 68–75.

Desmedt, C., Giobbie-Hurder, A., Neven, P., Paridaens, R., Christiaens, M.R., Smeets, A., Lallemand, F., Haibe-Kains, B., Viale, G., Gelber, R.D., et al. (2009). The Gene expression Grade Index: a potential predictor of relapse for endocrine-treated breast cancer patients in the BIG 1-98 trial. BMC Med. Genomics *2*, 40.

Eischen, C.M., Woo, D., Roussel, M.F., and Cleveland, J.L. (2001). Apoptosis triggered by Myc-induced suppression of Bcl-X(L) or Bcl-2 is bypassed during lymphomagenesis. Mol. Cell. Biol. *21*, 5063–5070.

Farmer, P., Bonnefoi, H., Anderle, P., Cameron, D., Wirapati, P., Becette, V., André, S., Piccart, M., Campone, M., Brain, E., et al. (2009). A stroma-related gene signature predicts resistance to neoadjuvant chemotherapy in breast cancer. Nat. Med. *15*, 68–74.

Feng, X., Arang, N., Rigiracciolo, D.C., Lee, J.S., Yeerna, H., Wang, Z., Lubrano, S., Kishore, A., Pachter, J.A., König, G.M., et al. (2019). A Platform of Synthetic Lethal Gene Interaction Networks Reveals that the GNAQ Uveal Melanoma Oncogene Controls the Hippo Pathway through FAK. Cancer Cell *35*, 457–472.e5.

Fruehauf, J.P. (2008). Axitinib (AG-013736) in patients with metastatic melanoma: a phase II study. Journal of Clinical Oncology *26*, 9006–9006.

Gide, T.N., Wilmott, J.S., Scolyer, R.A., and Long, G.V. (2018). Primary and Acquired Resistance to Immune Checkpoint Inhibitors in Metastatic Melanoma. Clin. Cancer Res. *24*, 1260–1270.

Graudens, E., Boulanger, V., Mollard, C., Mariage-Samson, R., Barlet, X., Grémy, G., Couillault, C., Lajémi, M., Piatier-Tonneau, D., Zaborski, P., et al. (2006). Deciphering cellular states of innate tumor drug responses. Genome Biol. *7*, R19.

Grimaldi, A.M., Simeone, E., Festino, L., Vanella, V., Strudel, M., and Ascierto, P.A. (2017). MEK Inhibitors in the Treatment of Metastatic Melanoma and Solid Tumors. Am. J. Clin. Dermatol. *18*, 745–754.

Guarneri, V., Dieci, M.V., Frassoldati, A., Maiorana, A., Ficarra, G., Bettelli, S., Tagliafico, E., Bicciato, S., Generali, D.G., Cagossi, K., et al. (2015). Prospective Biomarker Analysis of the Randomized CHER-LOB Study Evaluating the Dual Anti-HER2 Treatment With Trastuzumab and Lapatinib Plus Chemotherapy as Neoadjuvant Therapy for HER2-Positive Breast Cancer. Oncologist *20*, 1001–1010.

Han, J.-Y., Kim, H.Y., Lim, K.Y., Hwangbo, B., and Lee, J.S. (2016). A phase II study of nintedanib in patients with relapsed small cell lung cancer. Lung Cancer *96*, 108–112.

Hatzis, C., Pusztai, L., Valero, V., Booser, D.J., Esserman, L., Lluch, A., Vidaurre, T., Holmes, F., Souchon, E., Wang, H., et al. (2011). A genomic predictor of response and survival following taxane-anthracycline chemotherapy for invasive breast cancer. JAMA *305*, 1873–1881.

Hayashi, H., Takiguchi, Y., Minami, H., Akiyoshi, K., Segawa, Y., Ueda, H., Iwamoto, Y., Kondoh, C., Matsumoto, K., Takahashi, S., et al. (2020). Site-Specific and Targeted Therapy Based on Molecular Profiling by Next-Generation Sequencing for Cancer of Unknown Primary Site: A Nonrandomized Phase 2 Clinical Trial. JAMA Oncol. *6*, 1–9.

Horak, C.E., Pusztai, L., Xing, G., Trifan, O.C., Saura, C., Tseng, L.M., Chan, S., Welcher, R., and Liu, D. (2013). Biomarker analysis of neoadjuvant doxorubicin/cyclophosphamide followed by ixabepilone or Paclitaxel in early-stage breast cancer. Clin. Cancer Res. *19*, 1587–1595.

Huang, A.C., Orlowski, R.J., Xu, X., Mick, R., George, S.M., Yan, P.K., Manne, S., Kraya, A.A., Wubbenhorst, B., Dorfman, L., et al. (2019). A single dose of neoadjuvant PD-1 blockade predicts clinical outcomes in resectable melanoma. Nat. Med. *25*, 454–461.

Hugo, W., Shi, H., Sun, L., Piva, M., Song, C., Kong, X., Moriceau, G., Hong, A., Dahlman, K.B., Johnson, D.B., et al. (2015). Non-genomic and Immune Evolution of Melanoma Acquiring MAPKi Resistance. Cell *162*, 1271–1285.

Hugo, W., Zaretsky, J.M., Sun, L., Song, C., Moreno, B.H., Hu-Lieskovan, S., Berent-Maoz, B., Pang, J., Chmielowski, B., Cherry, G., et al. (2017). Genomic and Transcriptomic Features of Response to Anti-PD-1 Therapy in Metastatic Melanoma. Cell *168*, 542.

Hwang, S., Kwon, A.Y., Jeong, J.Y., Kim, S., Kang, H., Park, J., Kim, J.H., Han, O.J., Lim, S.M., and An, H.J. (2020). Immune gene signatures for predicting durable clinical benefit of anti-PD-1 immunotherapy in patients with non-small cell lung cancer. Sci. Rep. *10*, 643.

Iorio, F., Knijnenburg, T.A., Vis, D.J., Bignell, G.R., Menden, M.P., Schubert, M., Aben, N., Gonçalves, E., Barthorpe, S., Lightfoot, H., et al. (2016). A Landscape of Pharmacogenomic Interactions in Cancer. Cell *166*, 740–754.

Iwamoto, T., Bianchini, G., Booser, D., Qi, Y., Coutant, C., Shiang, C.Y., Santarpia, L., Matsuoka, J., Hortobagyi, G.N., Symmans, W.F., et al. (2011). Gene pathways associated with prognosis and chemotherapy sensitivity in molecular subtypes of breast cancer. J. Natl. Cancer Inst. *103*, 264–272.

Jansen, M.P., Knijnenburg, T., Reijm, E.A., Simon, I., Kerkhoven, R., Droog, M., Velds, A., van Laere, S., Dirix, L., Alexi, X., et al. (2013). Hallmarks of aromatase inhibitor drug resistance revealed by epigenetic profiling in breast cancer. Cancer Res. *73*, 6632–6641.

Julka, P.K., Chacko, R.T., Nag, S., Parshad, R., Nair, A., Oh, D.S., Hu, Z., Koppiker, C.B., Nair, S., Dawar, R., et al. (2008). A phase II study of sequential neoadjuvant gemcitabine plus doxorubicin followed by gemcitabine plus cisplatin in patients with operable breast cancer: prediction of response using molecular profiling. Br. J. Cancer *98*, 1327–1335.

Kakavand, H., Rawson, R.V., Pupo, G.M., Yang, J.Y.H., Menzies, A.M., Carlino, M.S., Kefford, R.F., Howle, J.R., Saw, R.P.M., Thompson, J.F., et al. (2017). PD-L1 Expression and Immune Escape in Melanoma Resistance to MAPK Inhibitors. Clin. Cancer Res. *23*, 6054–6061.

Katakami, N., Atagi, S., Goto, K., Hida, T., Horai, T., Inoue, A., Ichinose, Y., Koboyashi, K., Takeda, K., Kiura, K., et al. (2013). LUX-Lung 4: a phase II trial of afatinib in patients with advanced non-small-cell lung cancer who progressed

during prior treatment with erlotinib, gefitinib, or both. J Clin Oncol *31*, 3335–3341.

Kim, S.T., Cristescu, R., Bass, A.J., Kim, K.M., Odegaard, J.I., Kim, K., Liu, X.Q., Sher, X., Jung, H., Lee, M., et al. (2018). Comprehensive molecular characterization of clinical responses to PD-1 inhibition in metastatic gastric cancer. Nat. Med. *24*, 1449–1458.

Kiura, K., Nakagawa, K., Shinkai, T., Eguchi, K., Ohe, Y., Yamamoto, N., Tsuboi, M., Yokota, M., Seto, T., Jiang, H., et al. (2008). A randomized, double-blind, phase IIa dose-finding study of Vandetanib (ZD6474) in Japanese patients with non-small cell lung cancer. Journal of Thoracic Oncology *3*, 386–393.

Larkin, J., Chiarion-Sileni, V., Gonzalez, R., Grob, J.J., Cowey, C.L., Lao, C.D., Schadendorf, D., Dummer, R., Smylie, M., Rutkowski, P., et al. (2015). Combined nivolumab and ipilimumab or monotherapy in untreated melanoma. New England journal of medicine *373*, 23–34.

Law, V., Knox, C., Djoumbou, Y., Jewison, T., Guo, A.C., Liu, Y., Maciejewski, A., Arndt, D., Wilson, M., Neveu, V., et al. (2014). DrugBank 4.0: shedding new light on drug metabolism. Nucleic Acids Res. *42*, D1091–D1097.

Lee, J.S., and Ruppin, E. (2019). Multiomics Prediction of Response Rates to Therapies to Inhibit Programmed Cell Death 1 and Programmed Cell Death 1 Ligand 1. JAMA Oncol. *5*, 1614–1618.

Lee, J.S., Das, A., Jerby-Arnon, L., Arafeh, R., Auslander, N., Davidson, M., McGarry, L., James, D., Amzallag, A., Park, S.G., et al. (2018). Harnessing synthetic lethality to predict the response to cancer treatment. Nat. Commun. *9*, 2546.

Lisowska, K.M., Olbryt, M., Dudaladava, V., Pamuła-Piłat, J., Kujawa, K., Grzybowska, E., Jarząb, M., Student, S., Rzepecka, I.K., Jarząb, B., and Kupryjańczyk, J. (2014). Gene expression analysis in ovarian cancer - faults and hints from DNA microarray study. Front. Oncol. *4*, 6.

Liu, D., Schilling, B., Liu, D., Sucker, A., Livingstone, E., Jerby-Arnon, L., Zimmer, L., Gutzmer, R., Satzger, I., Loquai, C., et al. (2019). Integrative molecular and clinical modeling of clinical outcomes to PD1 blockade in patients with metastatic melanoma. Nat. Med. *25*, 1916–1927.

Lohrisch, C., Paltiel, C., Gelmon, K., Speers, C., Taylor, S., Barnett, J., and Olivotto, I.A. (2006). Impact on survival of time from definitive surgery to initiation of adjuvant chemotherapy for early-stage breast cancer. J Clin Oncol *24*, 4888–4894.

Lord, C.J., and Ashworth, A. (2017). PARP inhibitors: Synthetic lethality in the clinic. Science *355*, 1152–1158.

Magbanua, M.J., Wolf, D.M., Yau, C., Davis, S.E., Crothers, J., Au, A., Haqq, C.M., Livasy, C., Rugo, H.S., Esserman, L., et al. (2015). Serial expression analysis of breast tumors during neoadjuvant chemotherapy reveals changes in cell cycle and immune pathways associated with recurrence and response. Breast Cancer Res. *17*, 73.

Manojlovic, Z., Christofferson, A., Liang, W.S., Aldrich, J., Washington, M., Wong, S., Rohrer, D., Jewell, S., Kittles, R.A., Derome, M., et al. (2017). Comprehensive molecular profiling of 718 Multiple Myelomas reveals significant differences in mutation frequencies between African and European descent cases. PLoS Genet. *13*, e1007087.

Marcotte, R., Brown, K.R., Suarez, F., Sayad, A., Karamboulas, K., Krzyzanowski, P.M., Sircoulomb, F., Medrano, M., Fedyshyn, Y., Koh, J.L.Y., et al. (2012). Essential gene profiles in breast, pancreatic, and ovarian cancer cells. Cancer Discov. *2*, 172–189.

Marcotte, R., Sayad, A., Brown, K.R., Sanchez-Garcia, F., Reimand, J., Haider, M., Virtanen, C., Bradner, J.E., Bader, G.D., Mills, G.B., et al. (2016). Functional Genomic Landscape of Human Breast Cancer Drivers, Vulnerabilities, and Resistance. Cell *164*, 293–309.

Mariathasan, S., Turley, S.J., Nickles, D., Castiglioni, A., Yuen, K., Wang, Y., Kadel, E.E., III, Koeppen, H., Astarita, J.L., Cubas, R., et al. (2018). TGFβ attenuates tumour response to PD-L1 blockade by contributing to exclusion of T cells. Nature *554*, 544–548.

Miao, D., Margolis, C.A., Gao, W., Voss, M.H., Li, W., Martini, D.J., Norton, C., Bossé, D., Wankowicz, S.M., Cullen, D., et al. (2018). Genomic correlates of response to immune checkpoint therapies in clear cell renal cell carcinoma. Science *359*, 801–806.

Mok, T.S., Wu, Y.-L., Thongprasert, S., Yang, C.-H., Chu, D.-T., Saijo, N., Sunpaweravong, P., Han, B., Margono, B., Ichinose, Y., et al. (2009). Gefitinib or carboplatin–paclitaxel in pulmonary adenocarcinoma. New England Journal of Medicine *361*, 947–957.

Monika Belickova, M., Merkerova, M.D., Votavova, H., Valka, J., Vesela, J., Pejsova, B., Hajkova, H., Klema, J., Cermak, J., and Jonasova, A. (2016). Up-regulation of ribosomal genes is associated with a poor response to azacitidine in myelodysplasia and related neoplasms. Int. J. Hematol. *104*, 566–573.

Nathanson, T., Ahuja, A., Rubinsteyn, A., Aksoy, B.A., Hellmann, M.D., Miao, D., Van Allen, E., Merghoub, T., Wolchok, J.D., Snyder, A., and Hammerbacher, J. (2017). Somatic Mutations and Neoepitope Homology in Melanomas Treated with CTLA-4 Blockade. Cancer Immunol. Res. *5*, 84–91.

Newman, A.M., Liu, C.L., Green, M.R., Gentles, A.J., Feng, W., Xu, Y., Hoang, C.D., Diehn, M., and Alizadeh, A.A. (2015). Robust enumeration of cell subsets from tissue expression profiles. Nat. Methods *12*, 453–457.

Novello, S., Scagliotti, G.V., Rosell, R., Socinski, M.A., Brahmer, J., Atkins, J., Pallares, C., Burgess, R., Tye, L., Selaru, et al. (2009). Phase II study of continuous daily sunitinib dosing in patients with previously treated advanced non-small cell lung cancer. British journal of cancer *101*, 1543–1548.

Pathria, G., Lee, J.S., Hasnis, E., Tandoc, K., Scott, D.A., Verma, S., Feng, Y., Larue, L., Sahu, A.D., Topisirovic, I., et al. (2019). Translational reprogramming marks adaptation to asparagine restriction in cancer. Nat. Cell Biol. *21*, 1590–1603.

Pinyol, R., Montal, R., Bassaganyas, L., Sia, D., Takayama, T., Chau, G.Y., Mazzaferro, V., Roayaie, S., Lee, H.C., Kokudo, N., et al. (2019). Molecular predictors of prevention of recurrence in HCC with sorafenib as adjuvant treatment and prognostic factors in the phase 3 STORM trial. Gut *68*, 1065–1075.

Pires da Silva, I., Wang, K.Y.X., Wilmott, J.S., Holst, J., Carlino, M.S., Park, J.J., Quek, C., Wongchenko, M., Yan, Y., Mann, G., et al. (2019). Distinct Molecular Profiles and Immunotherapy Treatment Outcomes of V600E and V600K *BRAF*-Mutant Melanoma. Clin. Cancer Res. *25*, 1272–1279.

Pleasance, E., Titmuss, E., Williamson, L., Kwan, H., Culibrk, L., Zhao, E.Y., Dixon, K., Fan, K., Bowlby, R., Jones, M.R., et al. (2020). Pan-cancer analysis of advanced patient tumors reveals interactions between therapy and genomic landscapes. Nat. Cancer *1*, 452–468.

Prat, A., Navarro, A., Paré, L., Reguart, N., Galván, P., Pascual, T., Martínez, A., Nuciforo, P., Comerma, L., Alos, L., et al. (2017). Immune-Related Gene Expression Profiling After PD-1 Blockade in Non-Small Cell Lung Carcinoma, Head and Neck Squamous Cell Carcinoma, and Melanoma. Cancer Res. *77*, 3540–3550.

Reck, M., Rodríguez-Abreu, D., Robinson, A.G., Hui, R., Csoszi, T., Fülöp, A., Gottfried, M., Peled, N., Tafreshi, A., Cuffe, S., et al. (2016). Pembrolizumab versus chemotherapy for PD-L1–positive non–small-cell lung cancer. N engl J med *375*, 1823–1833.

Riaz, N., Havel, J.J., Makarov, V., Desrichard, A., Urba, W.J., Sims, J.S., Hodi, F.S., Martín-Algarra, S., Mandal, R., Sharfman, W.H., et al. (2017). Tumor and Microenvironment Evolution during Immunotherapy with Nivolumab. Cell *171*, 934–949.e16.

Ribas, A., Hamid, O., Daud, A., Hodi, F.S., Wolchok, J.D., Kefford, R., Joshua, A.M., Patnaik, A., Hwu, W.-J., Weber, J.S., et al. (2016). Association of pembrolizumab with tumor response and survival among patients with advanced melanoma. Jama *315*, 1600–1609.

Rizos, H., Menzies, A.M., Pupo, G.M., Carlino, M.S., Fung, C., Hyman, J., Haydu, L.E., Mijatov, B., Becker, T.M., Boyd, S.C., et al. (2014). BRAF inhibitor resistance mechanisms in metastatic melanoma: spectrum and clinical impact. Clin. Cancer Res. *20*, 1965–1977.

Rodon, J., Soria, J.C., Berger, R., Miller, W.H., Rubin, E., Kugel, A., Tsimberidou, A., Saintigny, P., Ackerstein, A., Braña, I., et al. (2019). Genomic and transcriptomic profiling expands precision cancer medicine: the WINTHER trial. Nat. Med. *25*, 751–758.

Rooney, M.S., Shukla, S.A., Wu, C.J., Getz, G., and Hacohen, N. (2015). Molecular and genetic properties of tumors associated with local immune cytolytic activity. Cell *160*, 48–61.

Roper, N., Brown, A.L., Wei, J.S., Pack, S., Trindade, C., Kim, C., Restifo, O., Gao, S., Sindiri, S., Mehrabadi, F., et al. (2020). Clonal Evolution and Heterogeneity of Osimertinib Acquired Resistance Mechanisms in EGFR Mutant Lung Cancer. Cell Rep. Med. *1*, 100007.

Sabine, V.S., Sims, A.H., Macaskill, E.J., Renshaw, L., Thomas, J.S., Dixon, J.M., and Bartlett, J.M. (2010). Gene expression profiling of response to mTOR inhibitor everolimus in pre-operatively treated post-menopausal women with oestrogen receptor-positive breast cancer. Breast Cancer Res. Treat. *122*, 419–428.

Sachdev, P., Hamid, O., Kim, K., Hauschild, A., O'Day, S.J., Andresen, C., Funahashi, Y., Kadowaki, T., O'Brien, J.P., and Flaherty, K. (2013). Analysis of serum biomarkers and tumor genetic alterations from a phase II study of lenvatinib in patients with advanced BRAF wild-type melanoma. Journal of Clinical Oncology *31*, 9058–9058.

Sahu, A.D., S Lee, J., Wang, Z., Zhang, G., Iglesias-Bartolome, R., Tian, T., Wei, Z., Miao, B., Nair, N.U., Ponomarova, O., et al. (2019). Genome-wide prediction of synthetic rescue mediators of resistance to targeted and immunotherapy. Mol. Syst. Biol. *15*, e8323.

Schalper, K.A., Rodriguez-Ruiz, M.E., Diez-Valle, R., López-Janeiro, A., Porciuncula, A., Idoate, M.A., Inogés, S., de Andrea, C., López-Diaz de Cerio, A., Tejada, S., et al. (2019). Neoadjuvant nivolumab modifies the tumor immune microenvironment in resectable glioblastoma. Nat. Med. *25*, 470–476.

Shi, L., Campbell, G., Jones, W.D., Campagne, F., Wen, Z., Walker, S.J., Su, Z., Chu, T.M., Goodsaid, F.M., Pusztai, L., et al.; MAQC Consortium (2010). The MicroArray Quality Control (MAQC)-II study of common practices for the development and validation of microarray-based predictive models. Nat. Biotechnol. *28*, 827–838.

Shi, Y., Zhang, L., Liu, X., Zhou, C., Zhang, L., Zhang, S., Wang, D., Li, Q., Qin, S., Hu, C., et al. (2013). Icotinib versus gefitinib in previously treated advanced non-small-cell lung cancer (ICOGEN): a randomised, double-blind phase 3 non-inferiority trial. The Lancet Oncology *14*, 953–961.

Snyder, A., Nathanson, T., Funt, S.A., Ahuja, A., Buros Novik, J., Hellmann, M.D., Chang, E., Aksoy, B.A., Al-Ahmadie, H., Yusko, E., et al. (2017). Contribution of systemic and somatic factors to clinical response and resistance to PD-L1 blockade in urothelial cancer: An exploratory multi-omic analysis. PLoS Med. *14*, e1002309.

Sorich, M.J., Pottier, N., Pei, D., Yang, W., Kager, L., Stocco, G., Cheng, C., Panetta, J.C., Pui, C.H., Relling, M.V., et al. (2008). In vivo response to methotrexate forecasts outcome of acute lymphoblastic leukemia and has a distinct gene expression profile. PLoS Med. *5*, e83.

Sosman, J.A., Kim, K.B., Schuchter, L., Gonzalez, R., Pavlick, A.C., Weber, J.S., McArthur, G.A., Hutson, T.E., Moschos, S.J., Flaherty, K.T., et al. (2012). Survival in BRAF V600-mutant advanced melanoma treated with vemurafenib. N Engl J Med *366*, 707–714.

Spentzos, D., Levine, D.A., Kolia, S., Otu, H., Boyd, J., Libermann, T.A., and Cannistra, S.A. (2005). Unique gene expression profile based on pathologic response in epithelial ovarian cancer. J. Clin. Oncol. *23*, 7911–7918.

Szklarczyk, D., Franceschini, A., Wyder, S., Forslund, K., Heller, D., Huerta-Cepas, J., Simonovic, M., Roth, A., Santos, A., Tsafou, K.P., et al. (2015). STRING v10: protein-protein interaction networks, integrated over the tree of life. Nucleic Acids Res. *43*, D447–D452.

Tanioka, M., Fan, C., Parker, J.S., Hoadley, K.A., Hu, Z., Li, Y., Hyslop, T.M., Pitcher, B.N., Soloway, M.G., Spears, P.A., et al. (2018). Integrated Analysis of RNA and DNA from the Phase III Trial CALGB 40601 Identifies Predictors of Response to Trastuzumab-Based Neoadjuvant Chemotherapy in HER2-Positive Breast Cancer. Clin. Cancer Res. *24*, 5292–5304.

Terragna, C., Remondini, D., Martello, M., Zamagni, E., Pantani, L., Patriarca, F., Pezzi, A., Levi, G., Offidani, M., Proserpio, I., et al. (2016). The genetic and genomic background of multiple myeloma patients achieving complete response after induction therapy with bortezomib, thalidomide and dexamethasone (VTD). Oncotarget *7*, 9666–9679.

Thompson, J.C., Hwang, W.T., Davis, C., Deshpande, C., Jeffries, S., Rajpurohit, Y., Krishna, V., Smirnov, D., Verona, R., Lorenzi, M.V., et al. (2020). Gene signatures of tumor inflammation and epithelial-to-mesenchymal transition (EMT) predict responses to immune checkpoint blockade in lung cancer with high accuracy. Lung Cancer *139*, 1–8.

Tsherniak, A., Vazquez, F., Montgomery, P.G., Weir, B.A., Kryukov, G., Cowley, G.S., Gill, S., Harrington, W.F., Pantel, S., Krill-Burger, J.M., et al. (2017). Defining a Cancer Dependency Map. Cell *170*, 564–576.e16.

Van Allen, E.M., Miao, D., Schilling, B., Shukla, S.A., Blank, C., Zimmer, L., Sucker, A., Hillen, U., Foppen, M.H.G., Goldinger, S.M., et al. (2015). Genomic correlates of response to CTLA-4 blockade in metastatic melanoma. Science *350*, 207–211.

Vaske, O.M., Bjork, I., Salama, S.R., Beale, H., Tayi Shah, A., Sanders, L., Pfeil, J., Lam, D.L., Learned, K., Durbin, A., et al. (2019). Comparative Tumor RNA Sequencing Analysis for Difficult-to-Treat Pediatric and Young Adult Patients With Cancer. JAMA Netw. Open *2*, e1913968.

Wakelee, H.A., Gettinger, S., Engelman, J., Jänne, P.A., West, H., Subramaniam, D.S., Leach, J., Wax, M., Yaron, Y., Miles, D.R., and Lara, P.N., Jr. (2017). A phase Ib/II study of cabozantinib (XL184) with or without erlotinib in patients with non-small cell lung cancer. Cancer chemotherapy and pharmacology *79*, 923–932.

Wei, S.C., Levine, J.H., Cogdill, A.P., Zhao, Y., Anang, N.A.S., Andrews, M.C., Sharma, P., Wang, J., Wargo, J.A., Pe'er, D., and Allison, J.P. (2017). Distinct Cellular Mechanisms Underlie Anti-CTLA-4 and Anti-PD-1 Checkpoint Blockade. Cell *170*, 1120–1133.e17.

Wherry, E.J., Ha, S.J., Kaech, S.M., Haining, W.N., Sarkar, S., Kalia, V., Subramaniam, S., Blattman, J.N., Barber, D.L., and Ahmed, R. (2007). Molecular signature of CD8+ T cell exhaustion during chronic viral infection. Immunity *27*, 670–684.

Whitfield, M.L., George, L.K., Grant, G.D., and Perou, C.M. (2006). Common markers of proliferation. Nat. Rev. Cancer *6*, 99–106.

Wong, M., Mayoh, C., Lau, L.M.S., Khuong-Quang, D.A., Pinese, M., Kumar, A., Barahona, P., Wilkie, E.E., Sullivan, P., Bowen-James, R., et al. (2020). Whole genome, transcriptome and methylome profiling enhances actionable target discovery in high-risk pediatric cancer. Nat. Med. *26*, 1742–1753.

Wongchenko, M.J., McArthur, G.A., Dréno, B., Larkin, J., Ascierto, P.A., Sosman, J., Andries, L., Kockx, M., Hurst, S.D., Caro, I., et al. (2017). Gene Expression Profiling in *BRAF*-Mutated Melanoma Reveals Patient Subgroups with Poor Outcomes to Vemurafenib That May Be Overcome by Cobimetinib Plus Vemurafenib. Clin. Cancer Res. *23*, 5238–5245.

Yarchoan, M., Hopkins, A., and Jaffee, E.M. (2017). Tumor Mutational Burden and Response Rate to PD-1 Inhibition. N. Engl. J. Med. *377*, 2500–2501.

Zhao, J., Chen, A.X., Gartrell, R.D., Silverman, A.M., Aparicio, L., Chu, T., Bordbar, D., Shan, D., Samanamud, J., Mahajan, A., et al. (2019). Immune and genomic correlates of response to anti-PD-1 immunotherapy in glioblastoma. Nat. Med. *25*, 462–469.

Please cite this article in press as: Lee et al., Synthetic lethality-mediated precision oncology via the tumor transcriptome, Cell (2021), https://doi.org/10.1016/j.cell.2021.03.030

STAR★METHODS

KEY RESOURCES TABLE

REAGENT or RESOURCE	SOURCE	IDENTIFIER
Software and algorithms		
SELECT	This study	https://zenodo.org/record/4661265
Deposited data		
The Cancer Genome Atlas	Cancer Genome Atlas Research et al., 2013	https://gdac.broadinstitute.org/
Project Achilles	Aguirre et al., 2016; Cheung et al., 2011; Cowley et al., 2014	https://depmap.org/portal/achilles/
DepMap	Tsherniak et al., 2017	https://depmap.org/portal/download/
Marcotte	Marcotte et al., 2012; Marcotte et al., 2016	https://depmap.org/portal/download/
Cancer Cell Line Encyclopedia	Barretina et al., 2012	https://portals.broadinstitute.org/ccle
Cancer Therapeutics Response Portal	Basu et al., 2013	https://www.broadinstitute.org/ctrp
Genomics of Drug Sensitivity in Cancer	Barretina et al., 2012	https://www.cancerrxgene.org/
Taxane treated ovarian cancer	Lisowska et al., 2014	GSE63885
5FU/Doxorubicin treated colorectal cancer	Iwamoto et al., 2011	GSE22093
Taxane/Anthracycline treated breast cancer	Hatzis et al., 2011	GSE25055
Doxorubicin/Paclitaxel treated breast cancer	Horak et al., 2013	GSE41998
Taxane/Anthracycline treated breast cancer	Magbanua et al., 2015	GSE32603
Paclitaxel treated breast cancer	Shi et al., 2010	GSE20194
Epirubicin treated breast cancer	Farmer et al., 2009	GSE4779
Taxane treated ovarian cancer	Spentzos et al., 2005	GSE31245
Irinotecan treated colorectal cancer	Graudens et al., 2006	GSE3964
Methotrexate treated leukemia	Sorich et al., 2008	GSE10255
Irinotecan treated colorectal cancer	Del Rio et al., 2017	GSE72970
Gemcitabine/Doxorubicin treated breast cancer	Julka et al., 2008	GSE8465
Anastrozole treated breast cancer	Jansen et al., 2013	GSE41994
Vemurafenib/Dabrafenib treated melanoma	Rizos et al., 2014	GSE50509
Vemurafenib/Dabrafenib treated melanoma	Hugo et al., 2015	GSE65185
Vemurafenib/Dabrafenib treated melanoma	Kakavand et al., 2017	GSE99898
Everolimus treated breast cancer	Sabine et al., 2010	GSE119262
Tamoxifen treated breast cancer	Desmedt et al., 2009	GSE16391
Lapatinib treated breast cancer	Guarneri et al., 2015	GSE66399
Bortezomib treated multiple myeloma	Terragna et al., 2016	GSE68871
Azacitidine treated myelodysplastic syndrome	Monika Belickova et al., 2016	GSE77750
Sorafenib treated liver cancer	Pinyol et al., 2019	GSE109211
Anti-PD1 treated non-small cell lung cancer	Cho et al., 2020	GSE126044
Anti-PD1 treated melanoma	Hugo et al., 2017	GSE78220
Anti-PD1 treated non-small cell lung cancer	Hwang et al., 2020	GSE136961
Anti-PD1 treated melanoma	Huang et al., 2019	GSE123728
Anti-PD1 treated non-small cell lung cancer	This study	GSE166449
Dexamethasone treated multiple myeloma	Manojlovic et al., 2017	https://gdc.cancer.gov/about-gdc/contributed-genomic-data-cancer-research/foundation-medicine/multiple-myeloma-research-foundation-mmrf
Gemtuzumab treated acute myeloid leukemia	Bolouri et al., 2018	https://ocg.cancer.gov/programs/target/projects/acute-myeloid-leukemia

(*Continued on next page*)

Continued

REAGENT or RESOURCE	SOURCE	IDENTIFIER
Drugbank	Law et al., 2014	https://go.drugbank.com/
STRING	Szklarczyk et al., 2015	https://string-db.org/
WINTHER trial	Rodon et al., 2019	http://www.winconsortium.org/clinical-trial/winther-trial1
Personalized Onco-Genomics	Pleasance et al., 2020	https://www.personalizedoncogenomics.org/cbioportal/
TEMPUS xT	Beaubier et al., 2019	https://search.vivli.org/doiLanding/studies/00004321/isLanding

RESOURCE AVAILABILITY

Lead contact

Further information and requests for resources and reagents should be directed to and will be fulfilled by the Lead Contact, Eytan Ruppin (eytan.ruppin@nih.gov).

Materials availability

This study did not generate new unique reagents.

Data and code availability

The transcriptomics profiles and treatment outcome information of the 23 publicly available clinical trials where SELECT is predictive and the custom code of our framework are available via ZENODO repository: https://zenodo.org/record/4661265. The data from the many of the remaining trials cannot be shared due to restrictions in the data sharing agreement. The accession number for the new SMC dataset (pembrolizumab-treated lung adenocarcinoma cohort) reported in this paper is GEO: GSE166449.

METHOD DETAILS

Data collection

We collected the cancer patients' tumor transcriptomics data with therapy response information from public databases. Our search was focused on GEO and ArrayExpress but also included a general literature search using different combinations of the following search terms: 'drug response, patient, cancer pre-treatment expression, transcriptomics, and therapy resistance' performed by March 2019 and with additional incoming datasets added as they became available to us thereafter (Braun et al., 2020; Cho et al., 2020; Damotte et al., 2019; Liu et al., 2019; Roper et al., 2020; Thompson et al., 2020). We focused on those clinical trial cohorts that have at least 5 responders and non-responders with sample size greater than 15. The collected cohorts include 13 chemotherapy, 14 targeted therapy (drugs of specific targets) and 21 immune checkpoint therapy cohorts covering a total of 13 cancer types treated with 32 drugs. The immune checkpoint therapy cohorts include a new unpublished dataset of lung adenocarcinoma patients treated with pembrolizumab at Samsung Medical Center. Among the entire collection of the 48 clinical trial cohorts, 23 datasets are accessible via ZENODO repository: https://zenodo.org/record/4661265.

The SELECT pipeline

Identifying SL/SR interaction partners of drug targets

Generating an initial pool of SL drug target interactions for targeted therapy. To identify clinically relevant SL interactions for targeted therapies, we followed the three-step procedure described in (Lee et al., 2018). (1) We created an initial pool of SL pairs identified in cell lines via RNAi/CRISPR-Cas9 (Aguirre et al., 2016; Cheung et al., 2011; Cowley et al., 2014; Marcotte et al., 2012; Marcotte et al., 2016) or pharmacological screens (Barretina et al., 2012; Basu et al., 2013; Iorio et al., 2016). For drug target gene T and candidate SL partner gene P, we checked whether the growth reduction induced by knocking out/down gene T or pharmacologically inhibiting gene T is stronger when gene P is inactive via a Wilcoxon rank-sum test. (2) Second, among the candidate gene pairs from the first step, we selected those gene pairs whose coinactivation is associated with better prognosis in patients, using a Cox proportional hazard model, testifying that they may thus hamper tumor progression. Third, we prioritized the SL paired genes with similar phylogenetic profiles across different species. Because of the distinct distribution of p values for the first two screens as shown in Figure S2, we performed a false discovery correction with 1% for the *in vitro* screen (1st step) and 10% for the tumor screen (2nd step). We were able to identify significant SL partners with these FDR thresholds for most of the datasets. However, for the cases where we did not find any significant SL partners with this set of FDR thresholds, we relaxed the FDR thresholds in two step manner to find the most significant set of SL partners; we first relaxed the FDR for the *in vitro* screen to 5% while keeping the FDR threshold for

Please cite this article in press as: Lee et al., Synthetic lethality-mediated precision oncology via the tumor transcriptome, Cell (2021), https://doi.org/10.1016/j.cell.2021.03.030

the tumor screening step at 10% (when analyzing GSE8465 and GSE3964). If this did not provide any significant pairs, we further relaxed both FDRs to 20% (when analyzing GSE16391, GSE41994, GSE68871). If we did not identify any significant pairs even with 20% FDR, we declared the corresponding drug as non-predictable by SELECT, as we could not reliably identify its candidate SL partners.

Generating compact biomarker SL signatures for targeted therapy. The number of SL partners that pass FDR ranges from 50 to 1,000 depending on the drugs and specific FDR thresholds. Among such candidate SL partners that pass above FDR thresholds, we further filtered these SL partners to generate a small set that is used to make the drug response predictions. This further filtering has been motivated by the following three reasons: (1) Occam's razor (regularization): predictor with a smaller number of variables are likely to generalize better. (2) Biomarker interpretability: Small sets of partners are more relevant for clinical use as predictive biomarkers. (3) Patient cohort comparative analysis: when comparing the SL-scores of different drugs to decide which would be the best fit for a given patient, using the same number of top predictors facilitates such an analysis on equal grounds. To determine the top significant SL partners, we performed a limited training on the BRAF inhibitor dataset (GSE50509) as shown in Figure S1A. Following the training, the number of top significant set size was set to 25 where the SL partners were ranked with their patient survival significance in TCGA data.

Generating the initial pool of SR drug target interactions for immunotherapy. To identify GIs for immunotherapy, we introduced a few modifications to our previously published GI inference pipelines (Lee et al., 2018; Sahu et al., 2019) to better capture the characteristics of immune checkpoint therapy. (1) For anti-PD1/PDL1 therapy, where the antibody blocks the physical interaction between PD1 and PDL1, we considered the interaction term (i.e., the product of *PD1* and *PDL1* gene expression values) to identify the SR partners of the treatment. For anti-CTLA4 therapy, where there the precise mechanism of action is less well characterized and involves several ligand/receptor interactions (Wei et al., 2017), we focused on the protein expression levels of CTLA4 (available via reverse phase protein lysate microarray (RPPA) values in TCGA data) as they are likely to better reflect the activity than the mRNA levels. (We have used the median CTLA4 protein expression for the samples where CTLA4 RPPA data is not available.) For anti-PD1/PDL1 therapy, we had to use gene expression rather than protein expression because protein expression of *PD1* and *PDL1* are not available for many samples. (2) For the GI partner levels, we resorted to their gene expression and somatic copy number alterations (SCNA) data as referenced in previous studies (Lee et al., 2018; Sahu et al., 2019) because protein expression was measured only for a small subset of genes. (3) Instead of considering all protein coding genes as candidates for SR partners, we focused on the genes that are covered by the NanoString panel (Table S4) because (i) the gene expression of many of immune checkpoint therapy datasets was quantified by NanoString platform and (ii) NanoString panel is enriched with immune system related genes that are highly relevant to the response to immune checkpoint therapy. (4) We omitted the first step of the SL/SR inference procedure, which is aimed at identifying candidate genetic interactions from the cell line functional screening data, because these interactions are not relevant to immune checkpoint response. We could in principle use the genome-wide CRISPR screens in cancer cell/T cell co-culture, but this data is limited to melanoma and the coverage is not fully genome-wide, where many genes included in the NanoString panel are missing. We kept all the remaining steps of the published SL/SR inference procedures. (5) We focused on the mediators of resistance to immune checkpoint therapies using synthetic rescue (SR) interactions, as no statistically significant SL interaction partners were identified via ISLE for either PD1/PDL1 or CTLA4.

Generating compact biomarker SR signatures for immunotherapy. To determine the top significant SR partners, we performed a limited training on (Van Allen et al., 2015) as shown in Figure S1B. Following the training, the number of top significant set size was set to 10 where the SR partners are ranked with their phylogenetic distances. These parameters were used in making all immune checkpoint therapy response predictions. We analyzed TCGA data applying this pipeline to identify pan cancer SR interactions that are more likely to be clinically relevant across many cancer types. In particular, we focused on the SR interactions where the inactivation of the target gene is compensated by the downregulation of the partner rescuer gene, as the other types of SR interactions introduced in (Sahu et al., 2019) were not predictive in the training dataset.

Predicting drug response in patients using SL/SR partners

We used the identified SL or SR partners for drug response prediction. We defined *SL-score* for chemotherapy and targeted therapy as the fraction of inactive SL partners in a given sample out of all SL partners of that drug. The SL-score reflects the intuitive notion that a targeted drug would be more effective when a larger fraction of its SL partners is inactive in the tumor. In each patient drug response dataset, a gene is determined to be inactive if its expression is below bottom tertile across samples in the same dataset, adhering to our previously published approaches (Lee et al., 2018; Sahu et al., 2019). We made this choice of normalization (i) to account for the basal expression level of each gene in specific tumor type and (ii) to minimize batch effects occurring when different datasets are combined. We additionally multiplied the SL-score by a target gene factor to obtain the final SL-score. This has been motivated by the notion that an inhibitor will not be effective when its target gene is not expressed; thus, we set the target gene factor to be zero when the target gene is inactive (below bottom 30-percentile in the given sample), and we used mean expression of the targets genes when the given drug has more than one target gene. Drug target genes were primarily mapped based on DrugBank (Law et al., 2014), and we referred other sources such as WINTHER trial and the literature with exception to the target genes whose mechanism of action is explicitly denoted in DrugBank as an agonist. The drug-to-target mapping used in our analysis can be found in Table S5. We used SR-score to predict response to immunotherapy, that quantifies the fraction *f*, SR partners that are inactive, and we used 1-*f* as the SR-score to predict responders. Higher SL- or SR-score is predictive of response to therapies.

Please cite this article in press as: Lee et al., Synthetic lethality-mediated precision oncology via the tumor transcriptome, Cell (2021), https://doi.org/10.1016/j.cell.2021.03.030

Using the computed SL/SR-scores, we studied SELECT's prediction accuracy in individual clinical trial cohorts. Overall, we used the entire relevant cohorts for our analysis to test the accuracy. There are several exceptions to this when we focus on a subset of the cohorts. For the cohorts that include both pre- and post-treatment biopsies, we naturally focused on pre-treatment biopsies (GSE8465, GSE32603, GSE50509, GSE65185, GSE99898, GSE77750, GSE119262, and the immunotherapy cohort (Nathanson et al., 2017)); for the cohorts composed of multiple treatments or placebo arms, we focused on the patients receiving the specific targeted therapy of interest (GSE72970, GSE3264, TARGET AML, MMRF, GSE16391, and GSE66399). The pertaining detailed information is available in Table S1 Column 'Criteria for subsetting samples.'

To define the responders and non-responders, we aimed to faithfully use the criteria defined in the original clinical trials as much as possible. For the datasets where the response information is available in the form of RECIST criteria, we solved a classification problem, quantifying the AUC of the pertaining ROC curve (rounded up to the second digit after the decimal point). For the cohorts where RECIST information is available, we used CR, PR as responders and SD, PD as non-responders (GSE63885, GSE41998, GSE72970, GSE3264 and the immunotherapy cohorts (Damotte et al., 2019; Gide et al., 2018; Hugo et al., 2017; Mariathasan et al., 2018; Miao et al., 2018; Nathanson et al., 2017; Prat et al., 2017; Thompson et al., 2020; Van Allen et al., 2015), and New SMC dataset). For the bortezomib cohort (GSE68871), we used CR, nCR as responders and PR, SD, VGPR as non-responders. For the cohorts where pathological clinical response (pCR) information is available, we used pCR as responders, and no-pCR as non-responders (GSE22093, GSE32603, GSE20194, GSE66399, and GSE4779). For the cohorts where response and non-response are defined by specific individual clinical trial cohorts, we followed the definition of the original cohorts (GSE31811, GSE8465, GSE50509, and immunotherapy cohorts (Chen et al., 2016; Cho et al., 2020; Huang et al., 2019; Kim et al., 2018)). For GSE77750, we used 'treatment' as responders and 'progressed','stable' as non-responders. For the immunotherapy cohort of (Hwang et al., 2020), we have used 'no recurrence' as responder and 'recurrence' as non-responder. For GSE119262, we have used a response metric based on Ki67, as used in the original study. For methotrexate (GSE10255), we have used the median white blood cell (WBC) change to define response, as was used in the original investigation. For (Braun et al., 2020), we used CR, PR, SD as responders (n = 8) and PD as non-responders (n = 8), which yields AUC = 0.77, since the number of CR/PR only was too small (n = 3); however, we confirmed that, even with taking CR/PR as responders (n = 3) and SD/PD as non-responders (n = 13) like other cohorts, SELECT is still predictive (AUC = 0.81). For the cases where progression-free survival time is available for all patients (with no censoring event), we used the median progression-free survival from the relevant literature as cutoff to distinguish the responders from non-responders and solved a classification problem. For BRAF inhibitor cohorts, we have used 7-month progression-free survival as criteria for response following the literature (Sosman et al., 2012). For GSE16391, we have used 75-percentile of the relapse-free survival (= 50 months; 6 responders and 17 non-responders) as threshold for response that is comparable with the reported values in the literature (Lohrisch et al., 2006); in this cohort, we also confirmed that the prediction accuracy is above 0.7 for a wide range of thresholds that separates responders versus non-responders including 4.8 years (the exact value reported in the literature). For the datasets where we only had the overall or progression-free survival with censoring information, we performed a Kaplan-Meier analysis. It is known that the response based on RECIST and patient survival does not necessarily correlate, and we thus evaluated SELECT's predictive performance in either term according to the available data. The pertaining detailed information is available in Table S1 Columns 'Criteria for R,' and 'Criteria for NR.' The mean SL-score is the mean value of the SL-scores across many different targeted therapies (the drugs that were used in the WINTHER trial (see Experimental Procedures section 'Retrospective analysis of the WINTHER trial' below)), which is assigned to each sample.

Samsung Medical Center anti-PD1-treated lung adenocarcinoma cohort

RNA was purified from formalin-fixed paraffin-embedded (FFPE) or fresh tumor samples using the AllPrep DNA/RNA Mini Kit (QIAGEN, USA). The RNA concentration and purity were measured using the NanoDrop and Bioanalyzer (Agilent, USA). The library was prepared following the manufacturer's instructions using the RNA Access Library Prep Kit (Illumina, USA). Tumor response was assessed by physicians using RECIST version 1.1 criteria. All 22 patients were treated with pembrolizumab, and all biopsy samples were obtained prior to the treatment.

TCGA anti-PD1 coverage analysis for predicting the cancer type-specific response to checkpoint therapy

To predict the objective response rates of anti-PD1 therapy in each cancer type in TCGA, we computed the SR scores of PD1 in each tumor sample based on each tumor's transcriptomics. We chose the point of maximal F1-score as the response classification threshold, computed across all anti-PD1/PDL1 datasets where the SR-score is predictive. Using this uniform threshold, we computed the fraction of responders for each cancer type. We then compared these predicted fractions of responders with the actual response rates reported in 16 anti-PD1 clinical trials (Yarchoan et al., 2017) using a Spearman rank correlation.

Retrospective analysis of the WINTHER trial

(1) The data: The trial involved 10 different cancer types, mostly colon, lung and head and neck cancer. It had two arms, one recommending treatment based on actionable mutations in a panel of cancer driver genes and the other based on the patients' transcriptomics data. We considered the Agilent microarray data of 71 patients with 50 different targeted treatments (single or combinations) that were available to us. One patient had a complete response, 7 had a partial response and 11 were reported to have stable disease (labeled as responders in our analysis), while 52 had a progressive disease (labeled as non-responders). To balance the size of

responders versus non-responders in this cohort, we defined CR/PR/SD as responders and PD as non-responders. (2) Inferring the SL partners of the drugs given in the cohort: For each of the drug that was used in the trial, we first identified their target genes' SL partners using SELECT. (3) Estimating the ability of SELECT to predict the patients' response to the drugs given: Based on the SL signatures, we used SELECT to calculate the SL-score of each therapy and quantified the prediction accuracy of all therapies given via a ROC analysis. We focused on the patients who received a single treatment (with less than two drug targets) since our subsequent analysis has focused on monotherapies. We note that, as expected, as the number of targets of a drug increases, its prediction accuracy decreases. (4) Charting the landscape of SL scores of all drugs across all patients: Lastly, to study the landscape of alternative treatment options recommended by SL-based approach, we considered all FDA-approved targeted therapies obtained from the DrugBank database (Law et al., 2014) and the literature as potential treatment candidates. The drug-to-target mapping used in our analysis can be found in Table S5. We then identified the SL partners of all the drugs' target genes and computed their SL-scores in each of the patient's based on their transcriptomic data and ranked them accordingly. The exact same procedure was used in the analysis of the TEMPUS cohort.

We additionally analyzed the post-treatment transcriptomics data together with treatment history from POG570 cohort (Pleasance et al., 2020). We normalized the RNaseq data following the same procedure described above for WINTHER trial data, and calculated SL-score for each sample using the treatments that the patients have received. We associated them with treatment duration, following its utilization as a proxy for treatment response in the original publication. We also compared the median treatment duration of high versus low SL-score patients (adhering to the choice of SL-score of 0.44 as classification threshold) across all patient-treatment pairs, and calculated the ratio between the median treatment duration of high versus low SL-score patients for each cancer type and each treatment of sample size greater than 15 patients.

Coverage analysis on TCGA data for melanoma and non-small-cell lung cancer

We collected relevant objective response rates (ORRs) for various clinical trials in melanoma (8 drugs) and non-small cell lung cancer (10 drugs) (Table S3) (Antonia et al., 2017; Brahmer et al., 2015; Daud et al., 2017; Decoster et al., 2010; Fruehauf, 2008; Han et al., 2016; Katakami et al., 2013; Kiura et al., 2008; Larkin et al., 2015; Lohrisch et al., 2006; Mok et al., 2009; Novello et al., 2009; Reck et al., 2016; Ribas et al., 2016; Sachdev et al., 2013; Shi et al., 2013; Wakelee et al., 2017). We excluded those clinical trials of combination therapies or of a small sample size (like those with a particular driver mutation). The number of patients participating in each clinical trial and the trial details are provided in Table S3.

We performed a coverage analysis on 356 TCGA melanoma or 981 TCGA non-small cell lung cancer patients using SELECT and predicted percentage of responders for each drug (using their drug targets). For predicting patient response, we used the threshold for SL/SR-scores to determine responders (i.e., a patient is a responder if SL-score > 0.44 for chemotherapy or targeted therapy; and SR-score ≥ 0.9 for immunotherapy). Then across the drugs within a given cancer type, we computed the Spearman's correlation between the fraction of responders in the respective TCGA cohorts (coverage) and the ORRs from clinical trials.

QUANTIFICATION AND STATISTICAL ANALYSIS

The receiver operating characteristics (ROC) and precision-recall analyses were performed using R library *ROCR*. Wilcoxon rank-sum test and Student's t test were performed using R functions *wilcox.test* and *t.test*, respectively. Gene Ontology (GO) enrichment analysis was performed using R library *topGO*. Statistical details of each clinical trial dataset can be found in Table S1. The Kaplan-Meier analysis was performed, where the effect size was measured by the median survival differences (or 80-percentile survival differences if survival exceeds 50% at the longest time point) and the corresponding significance was quantified by logrank test using R libraries, *survival* and *survminer*. All boxplots follow the standard definition, where the box is drawn from top quartile (75th percentile) to bottom quartile (25th percentile) of the data with a horizontal line drawn in the middle to denote the median value. The lowest point of the bottom whisker is the minimum of the data and the highest point of the top whisker is the maximum of the data.

ADDITIONAL RESOURCES

The clinical trial data and the source code are accessible for academic purposes via ZENODO repository: https://zenodo.org/record/4661265.

Supplemental figures

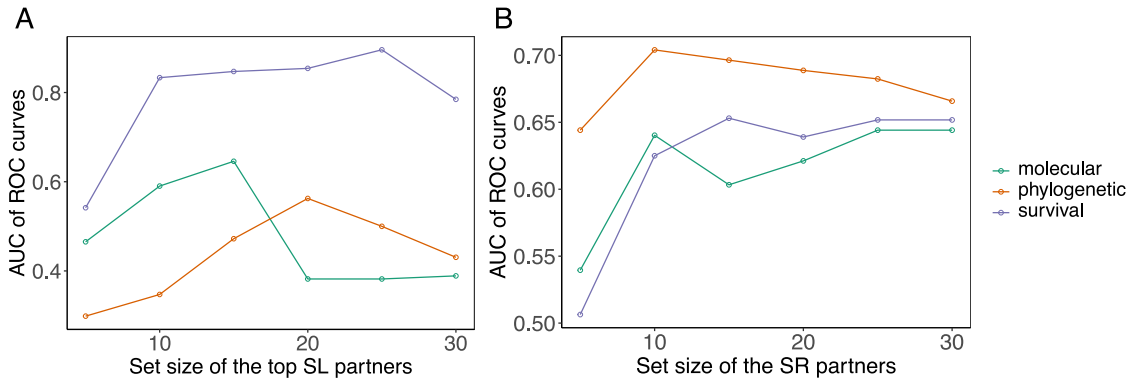

Figure S1. Determining the group size and ranking of the SL/SR partners of the SELECT framework, related to Figure 1

The top significant SL and SR partners used in the prediction of cytotoxic/targeted agents and immunotherapy were determined by varying the set sizes and ranking scheme in GSE50509 (Rizos et al., 2014) (cytotoxic and targeted) and Van Allen cohort (Van Allen et al., 2015) (immunotherapy), which are the datasets we initially started our analysis with, and determining the resulting prediction performance on these datasets. Based on this procedure, we selected 25 as the SL partners set size and the patient survival p values as the ranking scheme used in the analysis of all other cytotoxic/targeted agents and 10 as set size of the SR partners and phylogenetic score as the ranking scheme used for predicting the response for immune checkpoint immunotherapy.

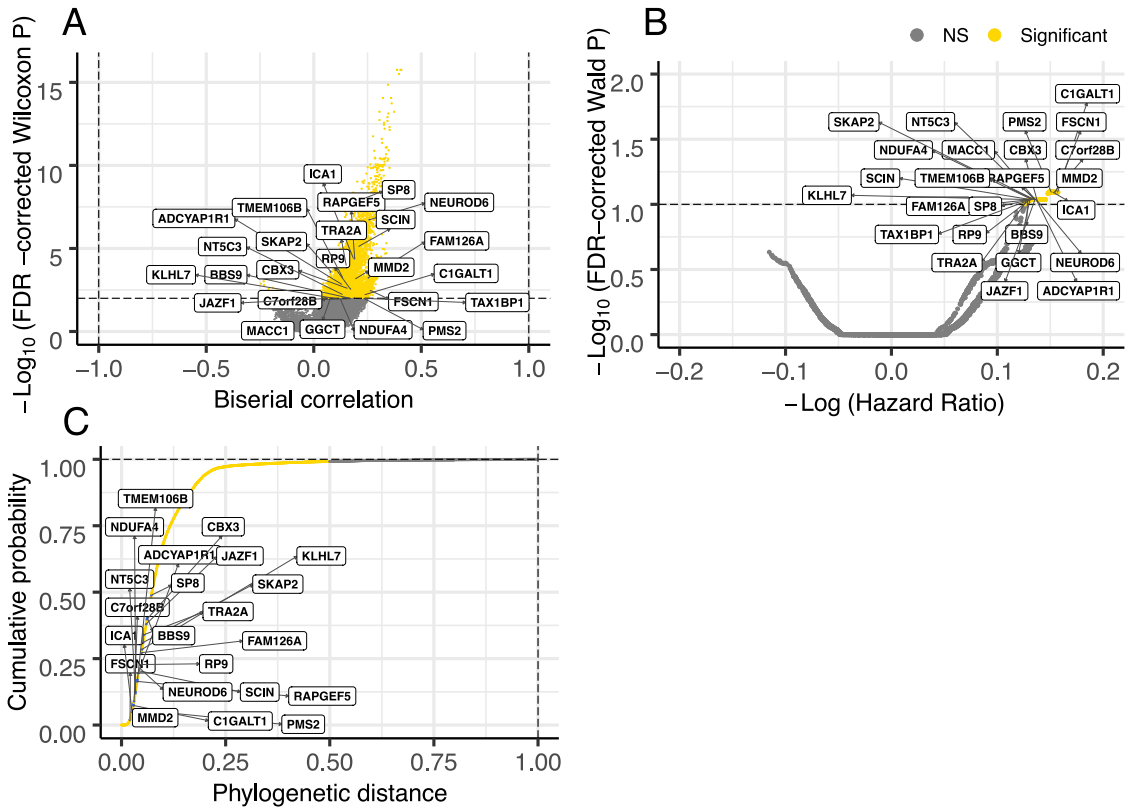

Figure S2. Distribution of the effect size and p values of the 25 identified BRAF SL partners across the three steps of the SELECT framework, related to Figures 1 and 2

This figure provides the rationale for determining the false discovery rates for SL inference. (A) The results of the first step of the SL screens. The volcano plot shows the point-biserial correlation coefficient (x axis) and Wilcoxon rank-sum p values (y axis) of all protein coding genes from *in vitro* RNAi/CRISPR-Cas9 screen and pharmacological inhibitions. For each candidate SL pair between the drug target (gene T; BRAF in this case) and the partner (gene P), we checked whether the growth defect induced by gene knock-out/down or pharmacological inhibition of gene T is stronger when gene P is inactive either by mRNA expression or somatic copy number alteration (SCNA). (B) The results of the second step of SL screen from TCGA tumor data. The volcano plot shows the Cox hazard ratio (x axis) and corresponding Wald p values (y axis), where we checked whether co-inactivation of gene P and T leads to significantly enhanced patient survival in TCGA data as described in (Lee et al., 2018). Note that the significance level is considerably lower for tumor screen compared to the *in vitro* screen. We thus used more stringent FDR correction for *in vitro* screen (1%) than tumor screen (10%). (C) The results from phylogenetic screen showing the cumulative distribution of (rank-normalized) phylogenetic distances between BRAF and all protein coding genes. The cutoff of 50-percentile was used following (Lee et al., 2018). The 25 identified BRAF SL partners are denoted in the figures.

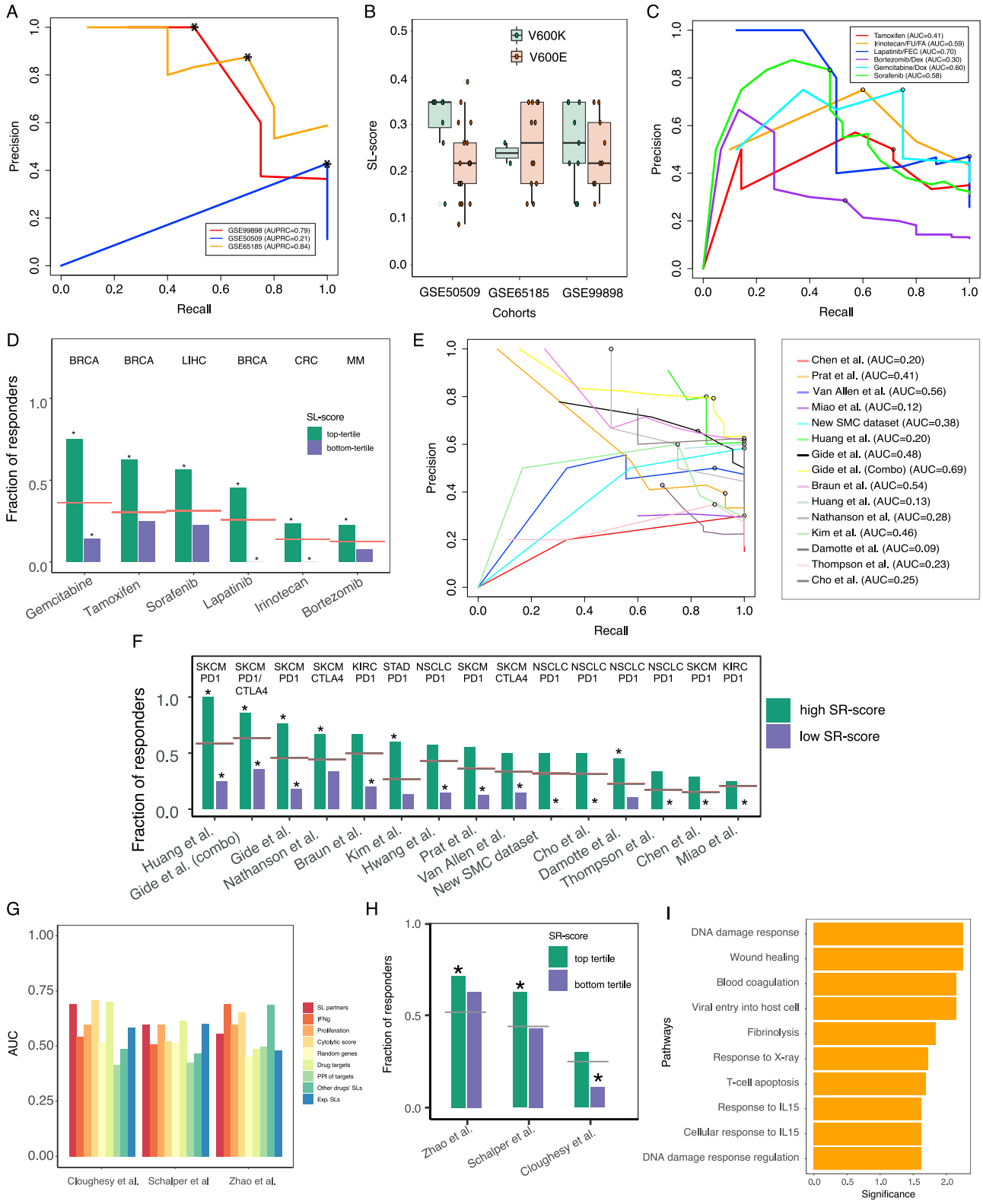

Figure S3. SELECT predicts response to cytotoxic agents, targeted therapy, and immunotherapy, related to Figures 3, 4, and 5

(A) Precision-recall curves depicting the prediction accuracy of the response to BRAF inhibitor using SL-scores in the three melanoma cohorts. (B) BRAF mutation status is not associated with SL-score. The SL-scores (y axis) of BRAF V600E mutated patients (red) versus BRAF V600K mutated patients (green) in three

(legend continued on next page)

melanoma cohorts GSE50509, GSE65185, and GSE99898 (x axis). Wilcoxon p values are 0.16, 0.87, and 0.51, respectively. (C) Precision-recall curves of other cytotoxic agents and targeted therapies. The AUC of each precision-recall curve is denoted in the figure legend, and the circles denote the point of maximal F1-score. (D) Bar graphs showing the fraction of responders in the patients with high SL-scores (top tertile; green) and low SL-scores (bottom tertile; purple). The gray line denotes the response rate in each cohort, and the stars denote the hypergeometric significance of enrichment of responders in the high-SL group and non-responders in the low-SL group. (E) Precision-recall curves for the SR-scores across the 15 different datasets with AUCs > 0.7. The AUC of each precision-recall curve is denoted in the figure legend, and the circles denote the point of maximal F1-score. (F) Bar graphs showing the fraction of responders in the patients with high SR-scores (top tertile; green) and low SR-scores (bottom tertile; purple). The gray line denotes the response rate in each cohort, and the stars denote the hypergeometric significance of enrichment of responders in the high-SR group and non-responders in the low-SR group. (G) Bar graphs show the predictive accuracy in terms of AUC (y axis) of SR-based predictors and control predictors across the three glioma cohorts (x axis). (control predictors are similar to those described in Figure 2C in the main text.) (H) Bar graphs showing the fraction of responders in the patients with high SR-scores (top tertile; green) and low SR-scores (bottom tertile; purple) in the three glioma datasets. The gray line denotes the response rate in each cohort, and the stars denote the hypergeometric significance of enrichment of responders in the high-SR group and non-responders in the low-SR group. (I) The bar graph of pathway enrichment analysis of 10 PD1-PDL1 and 10 CTLA4 SR partner genes in aggregate. x axis shows the $-\log_{10}$ (Fisher exact test p value) and y axis shows the enriched pathways.

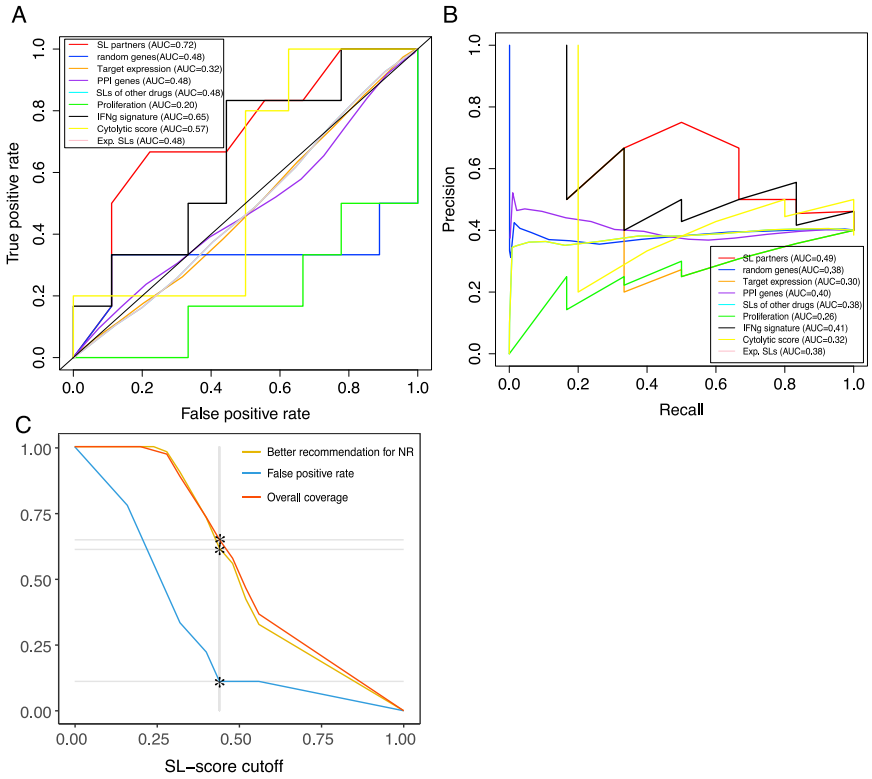

Figure S4. Predicting therapy response across different drugs and tumor types in WINTHER trial data, related to Figure 7

(A) The ROC plots show that the SL-scores are most predictive of response to the different treatments prescribed at the trial (AUC of ROC = 0.72), markedly higher than those of control predictors (as described in Figure 2C). (B) The parallel precision-recall, showing that the SL-score predictor outperforms an array of other control predictors (AUPRC = 0.49). (C) The x axis shows the SL-score classification threshold and y axis depicts the false positive rate (derived from the ROC curve presented in Figure 7B, (blue)), the overall coverage (the fraction of the patients in the WINTHER cohort for whom SELECT recommends higher SL-scoring alternate treatment options than those they have actually received, red), and the fraction of the non-responders in WINTHER cohort for whom SELECT recommends such treatment options (orange). As the SL-score decision threshold increases, less and less patients are denoted 'positive' (i.e., are assigned a treatment recommendation). At SL-score threshold of 0.44, SELECT recommends alternate treatments that are predicted to be effective for 65% of the entire cohort and 62% of non-responders (as marked by the stars).

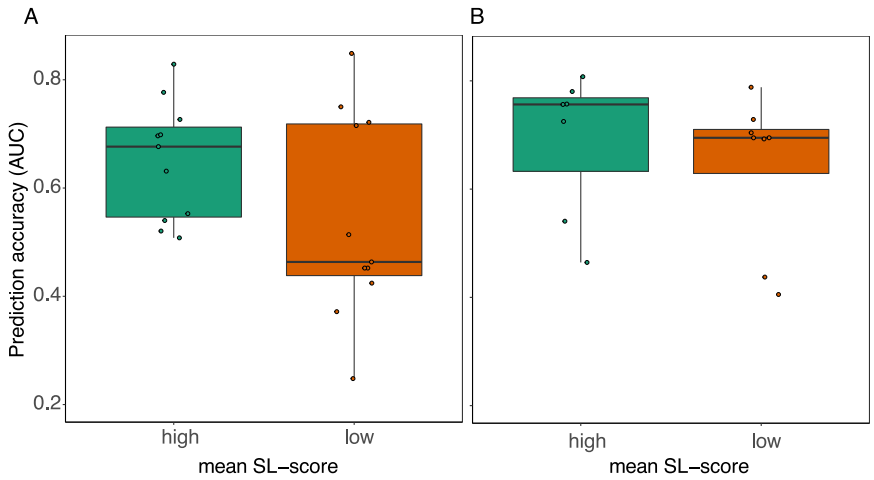

Figure S5. SELECT prediction accuracy versus mean SL-score, related to Figure 7

SELECT's prediction accuracy (AUCs) were compared between the cohorts where the mean SL-score is high (green) versus low (red, separated by median values of the mean SL-score). SELECT prediction accuracy is associated with the mean SL-score (**A**) for targeted therapy (Wilcoxon rank-sum $p < 0.06$) but (**B**) while a similar trend is also observed for immunotherapy, it is not significant (Wilcoxon rank-sum $p < 0.15$).

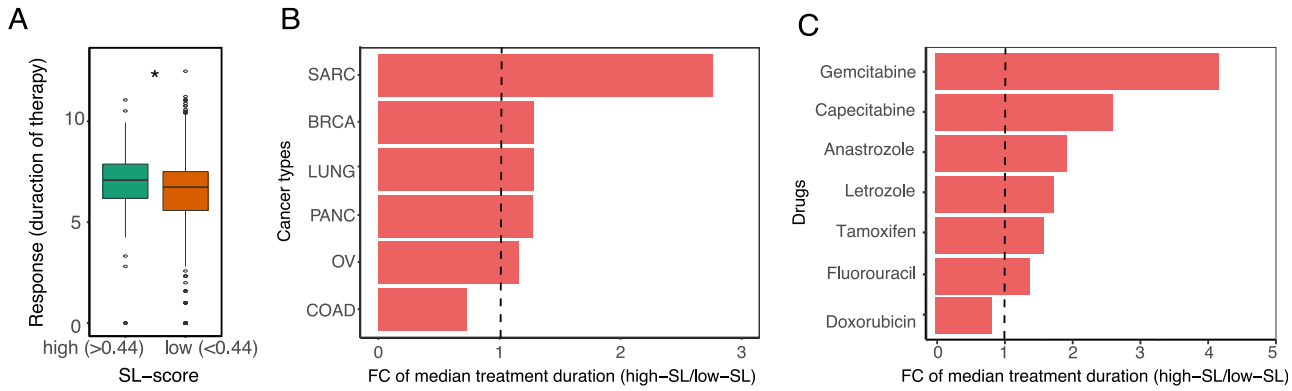

Figure S6. Predicting therapy response across different drugs and tumor types in POG570 trial data, related to Figure 7

(A) The SL-score is associated with treatment duration in the POG570 cohort (Wilcoxon rank-sum $p < 0.023$). (B-C) The fold change (FC) of median treatment duration in high SL-score group (SL-score > 0.44) versus low SL-score group (SL-score $\leq$ 0.44) for (B) each cancer type and (C) each drug, across all categories with more than 15 patients.

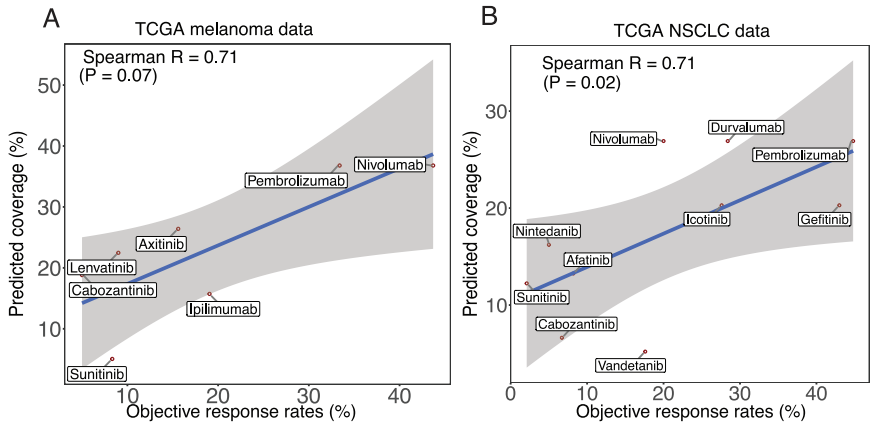

Figure S7. Coverage predicted by SL-score across different therapies in melanoma and lung cancer, related to Figure 7 and Table S3

SELECT is predictive of coverage (fraction of the patients predicted to be responsive to the given treatment based on the criteria, SL-score > 0.44 for targeted therapies and SR-score $\geq$ 0.9 for immunotherapies) across different therapies in (A) melanoma and (B) non-small cell lung cancer. Spearman rank correlation and associated p values are noted in the figures.